KKL Observer Synthesis for Nonlinear Systems via Physics-Informed Learning ⋆

M. Umar B. Niazi [a], John Cao [b], Matthieu Barreau [a], Karl Henrik Johansson [a]

[a] *Division of Decision and Control Systems, Digital Futures, KTH Royal Institute of Technology, SE-100 44 Stockholm, Sweden*

[b] *Department of Engineering Science, University of Oxford, Parks Road, Oxford, OX1 3PJ, UK*

Abstract

This paper proposes a novel learning approach for designing Kazantzis-Kravaris/Luenberger (KKL) observers for autonomous nonlinear systems. The design of a KKL observer involves finding an injective map that transforms the system state into a higher-dimensional observer state, whose dynamics is linear and stable. The observer's state is then mapped back to the original system coordinates via the inverse map to obtain the state estimate. However, finding this transformation and its inverse is quite challenging. We propose learning the forward mapping using a physics-informed neural network, and then learning its inverse mapping with a conventional feedforward neural network. Theoretical guarantees for the robustness of state estimation against approximation error and system uncertainties are provided, including non-asymptotic learning guarantees that link approximation quality to finite sample sizes. The effectiveness of the proposed approach is demonstrated through numerical simulations on benchmark examples, showing superior generalization capability outside the training domain compared to state-of-the-art methods.

Key words: Nonlinear systems, state estimation, KKL observers, physics-informed learning.

1 Introduction

Observers play a crucial role in applications such as output feedback control [49], fault diagnosis [18], and digital twins [19]. Accurate state estimation is critical for effective control, monitoring, and decision-making in various engineering domains. Full-state measurement of real-world systems is often impractical, or even impossible, due to limitations in sensing resources and capabilities. This necessitates the use of observers that employ available sensor measurements and the system's model to estimate the state.

A variety of observer designs exist, including Luenberger-like observers, extended Kalman filters, and high-gain observers, each with its own strengths and weaknesses depending on the specific application and system characteristics [9, 13, 24, 28]. This work focuses on Kazantzis-Kravaris/Luenberger (KKL) observers due to their applicability

⋆ This work is supported by the European Union's Horizon Research and Innovation Programme under Marie Skłodowska-Curie grant agreement No. 101062523. It has also received funding from the Swedish Research Council and the Knut and Alice Wallenberg Foundation, Sweden. Corresponding author: M. U. B. Niazi.

Email addresses: mubniazi@kth.se (M. Umar B. Niazi), john.cao@oriel.ox.ac.uk (John Cao), barreau@kth.se (Matthieu Barreau), kallej@kth.se (Karl Henrik Johansson).

to a very general class of nonlinear systems and the well-developed theoretical framework for their design and analysis [2, 4, 11, 14, 27].

Despite the advancements, synthesizing KKL observers remains a challenging task. The existing techniques assume the knowledge of an injective map that transforms a general nonlinear system into a special form required by the KKL observer. However, analytically finding this map is inherently difficult. Moreover, when this transformation map is known [10], finding its inverse to obtain the state estimate in the original, physically meaningful coordinates is also a difficult problem [3]. This highlights the need for novel approaches that can overcome these limitations.

In this paper, we present a novel learning approach for designing KKL observers for autonomous nonlinear systems. At the core of KKL observer design is an injective coordinate transformation that lifts the nonlinear system to a higher-dimensional space. The transformed system exhibits two key properties: its dynamics is bounded-input-bounded-state stable and linear up to output injection. The KKL observer operates by replicating the transformed system in the higher-dimensional space. To reconstruct the state estimate in the original coordinates, the left inverse of the transformation map is applied to the observer's state. The transformation map's injectivity property guarantees the accuracy of the state estimate.

Given a KKL observer in an appropriate high-dimensional space, the transformation map is a solution to a specific partial differential equation (PDE), [4, 27]. However, this PDE is computationally challenging to solve in practice, and finding the left inverse of the transformation map in real time is further challenging. To address these challenges, we develop a framework for learning these maps using synthetic data generated from system dynamics and sensor measurements. We employ physics-informed neural networks (PINNs) to directly integrate the PDE constraint into the learning process for the transformation map and its inverse.

This paper makes several key contributions to the learning-based design and implementation of KKL observers. We propose a physics-informed learning method for designing KKL observers and establish theoretical learning guarantees for this approach. Additionally, we provide robustness guarantees for the learned KKL observer against approximation errors and system uncertainties. Through extensive numerical simulations, we validate the effectiveness of our learning-based approach to KKL observer design and provide comparisons with state-of-the-art approaches.

The rest of the paper is organized as follows. Section 2 provides background and related literature on KKL observers and situates our work within the existing literature. Section 3 reviews the theoretical foundations of KKL observers. Section 4 reviews relevant notions in machine learning theory. In Section 5, we present our learning method for KKL observer design, followed by Sections 6 and 7, which develop theoretical learning and robustness guarantees, respectively. The effectiveness of our approach is demonstrated through numerical examples and comparisons in Section 8. Finally, Section 9 concludes the paper with a discussion of implications and future research directions.

2 Background and Related Literature

KKL observers generalize the theory of Luenberger observers [32–34] to nonlinear systems. Although the idea was initially proposed in [45] and [46], KKL observers were subsequently rediscovered by Kazantis and Kravaris [27], who provided local guarantees around an equilibrium point of the estimation error dynamics via Lyapunov's Auxiliary Theorem. Later, [30] relaxed the restrictive assumptions of [27] to some extent; however, the analysis remained local until [29] proposed the first global result under the assumption of so-called finite complexity, which also proved quite restrictive for general systems. Subsequently, Andrieu and Praly [4] provided a comprehensive treatment of the KKL observer problem. Their key contribution lies in relating the existence of an injective KKL transformation map to an observability-like property of the system known as backward distinguishability. In addition, [2] proved that KKL observers converge exponentially and are tunable if the system is also differentially observable. The existence

conditions are further refined in [14], and KKL observers with contracting dynamics are developed in [40]. When the observability conditions are not satisfied, [12] proposes a set-valued KKL observer that estimates a set of possible state trajectories that could have produced the observed output trajectories. Finally, extensions of KKL observers to non-autonomous and controlled nonlinear systems are presented in [8, 10, 22]; however, such systems are beyond the scope of the present paper.

The main challenge in synthesizing KKL observers for autonomous nonlinear systems is not only finding the transformation map that puts the system into a normal form, but also finding its inverse map. Both problems turn out to be challenging in practice. To this end, [15, 36, 39, 41, 42, 44, 50] have proposed several methods to approximate the transformation map and its inverse via deep neural networks.

By fixing the dynamics of the KKL observer, [44] proposes generating synthetic data trajectories by numerically integrating the system model and the KKL observer, both initialized at multiple points in their respective state spaces. Then, using a supervised learning approach, a neural network is trained on the synthetic data to approximate the transformation map and its left inverse. For discrete-time nonlinear systems, [41] proposes an unsupervised learning approach that enables proper exploration of the state space during training, whereas [42] extends this approach by allowing switching observers. However, noisy measurements can lead to erroneous switching decisions, causing the observer to select the wrong observer mode or introduce instability due to chattering. Similarly, [15] proposes another unsupervised learning approach for tuning a KKL observer while adding the PDE associated with the transformation map as a design constraint. The unsupervised approach exhibits poor generalization capabilities. Specifically, when the real system's initial state deviates significantly from the conditions observed during training, the observer's performance deteriorates considerably. When the system dynamics are partially or fully unknown, [36] proposes a neural ODE-based approach to design KKL observers, enabling analysis of the trade-off between convergence speed and robustness and leading to improved observer training for robust performance.

Our prior work [39] leveraged physics-informed learning to design KKL observers with improved generalization and training efficiency, and [16] used this approach for detecting and isolating sensor faults. In contrast to other learning-based approaches, we demonstrated that our method avoids overfitting and achieves better generalization performance across the entire state space. However, [39] employed a joint encoder-decoder neural network architecture to simultaneously learn the transformation map and its inverse, leading to conflicting gradients across components of the objective function. This causes the optimization to sometimes get stuck in a bad local minimum, which degrades the observer's accuracy in some instances [42]. In our current work, we introduce a sequential learning approach for the KKL observer. We first learn the transformation map and subsequently utilize it to learn its inverse. This approach improves the observer's accuracy by avoiding conflicting gradients during training. Furthermore, we provide theoretical non-asymptotic generalization bounds for the learned maps and prove that the resulting state estimation error is input-to-state stable with respect to approximation errors, model uncertainties, and measurement noise.

3 Preliminaries on KKL Observers

3.1 Notation

For $v \in \mathbb{R}^n$, $\|v\|$ denotes its Euclidean norm and $\|v\|_\infty$ its max norm. For a matrix $M \in \mathbb{R}^{m\times n}$, $\|M\|$ denotes its spectral norm and $\mathrm{cond}(M)$ its condition number. For a square matrix $M \in \mathbb{R}^{n\times n}$, $\mathrm{eig}(M) \subset \mathbb{C}$ denotes the set of its eigenvalues and $\lambda_{\min}(M) \in \min_{\lambda\in\mathrm{eig}(M)} |\mathrm{Re}(\lambda)|$ denotes an eigenvalue of M closest to the imaginary axis. We denote the set $[p] \coloneqq \{1, \dots, p\}$ for some $p \in \mathbb{Z}_{>0}$. Given a signal $s : \mathbb{R}_{\geq 0} \to \mathbb{R}^n$, we denote its restriction to $[0, t]$ by $s_{[0,t]}$, where $t \in \mathbb{R}_{\geq 0}$. Moreover, its essential supremum (or L_∞) norm is defined as $\|s_{[0,t]}\|_{L_\infty} \coloneqq \inf\{c \in \mathbb{R}_{\geq 0} : \|s(\tau)\|_\infty \leq c \text{ for almost all } \tau \in [0, t]\}$.

3.2 State Observation Problem

Consider a compact set $\mathcal{X} \subset \mathbb{R}^{n_x}$ and a nonlinear system

$$\dot{x}(t) = f(x(t)), \quad x(0) = x_0 \tag{1a}$$
$$y(t) = h(x(t)) \tag{1b}$$

where $x(t) \in \mathcal{X}$ is the state at time $t \in \mathbb{R}_{\geq 0}$, $x_0 \in \mathcal{X}$ is an *unknown* point from where the system's state is initialized, $y(t) \in \mathbb{R}^{n_y}$ is the *measured* output, and $f : \mathcal{X} \to \mathbb{R}^{n_x}$ and $h : \mathcal{X} \to \mathbb{R}^{n_y}$ are smooth functions. The state observation problem involves designing an *observer*

$$\dot{\hat{z}}(t) = \Phi(\hat{z}(t), y(t)), \quad \hat{z}(0) = \hat{z}_0 \tag{2a}$$
$$\hat{x}(t) = \Psi(\hat{z}(t), y(t)) \tag{2b}$$

with an internal state $\hat{z}(t) \in \mathbb{R}^{n_z}$ initialized at $\hat{z}_0 \in \mathbb{R}^{n_z}$, which takes the output $y(t)$ of (1) as its input and provides an estimate $\hat{x}(t) \in \mathbb{R}^{n_x}$ of the state $x(t)$ as its output. Designing an observer means choosing functions $\Phi : \mathbb{R}^{n_z} \times \mathbb{R}^{n_y} \to \mathbb{R}^{n_z}$ and $\Psi : \mathbb{R}^{n_z} \times \mathbb{R}^{n_y} \to \mathbb{R}^{n_x}$ so that the estimation error

$$\xi(t) \coloneqq x(t) - \hat{x}(t) \tag{3}$$

globally asymptotically converges to zero as $t \to \infty$. That is, for all $x_0 \in \mathcal{X}$ and $\hat{z}_0 \in \mathbb{R}^{n_z}$,

$$\lim_{t \to \infty} \|\xi(t)\| = 0. \tag{4}$$

3.3 KKL Observer

Designing a KKL observer involves transforming the nonlinear system (1) to a higher-dimensional state space where its dynamics is linear up to output injection and bounded-input bounded-state stable. This transformation $\mathcal{T} : \mathcal{X} \to \mathcal{Z}$, which must be injective [1], maps every point x in the state space $\mathcal{X} \subseteq \mathbb{R}^{n_x}$ of (1) to a point $z = \mathcal{T}(x)$ in the new state space $\mathcal{Z} \subseteq \mathbb{R}^{n_z}$, where in general $n_z \gg n_x$. The dynamics in the new state space $\mathcal{Z}$ is linear up to output injection and given by

$$\dot{z}(t) = Az(t) + Bh(x(t)), \quad z(0) = \mathcal{T}(x_0) \tag{5}$$

where $A \in \mathbb{R}^{n_z \times n_z}$ and $B \in \mathbb{R}^{n_z \times n_y}$ are chosen such that A is Hurwitz and the pair (A, B) is controllable [2]. Although the transformed system (5) in the new coordinates is stable, the original nonlinear system (1) need not be (Lyapunov) stable. Moreover, (5) is not a linear system, but its linearity is only up to output injection, i.e., it is linear when the injected output $y = h(x) = h(\mathcal{T}^*(z))$ is ignored, where $\mathcal{T}^*$ is the left-inverse of $\mathcal{T}$.

Since $\dot{z}(t) = \frac{\partial \mathcal{T}}{\partial x}(x(t))\dot{x}(t)$, it follows from (5) that, for a given A and B, $\mathcal{T}$ must satisfy the following PDE:

$$\frac{\partial \mathcal{T}}{\partial x}(x(t))f(x(t)) = A\mathcal{T}(x(t)) + Bh(x(t)) \tag{6}$$

with $\mathcal{T}(0_{n_x}) = 0_{n_z}$.

---

[1] A map $\mathcal{T} : \mathcal{X} \to \mathbb{R}^{n_z}$ is said to be *injective* if, for every $x_1, x_2 \in \mathcal{X}$, $\mathcal{T}(x_1) = \mathcal{T}(x_2)$ implies $x_1 = x_2$.

[2] (A, B) is controllable iff rank $\begin{bmatrix} B & AB & \dots & A^{n_z - 1}B \end{bmatrix} = n_z$.

To obtain a state estimate $\hat{x}(t)$ in the original coordinates $\mathbb{R}^{n_x}$, the map $\mathcal{T}$ must be injective, implying the existence of its left inverse $\mathcal{T}^*$, i.e., $\mathcal{T}^*(\mathcal{T}(x)) = x$. When this inverse exists, the KKL observer is obtained as

$$\dot{\hat{z}}(t) = A\hat{z}(t) + By(t), \quad \hat{z}(0) = \hat{z}_0 \tag{7a}$$
$$\hat{x}(t) = \mathcal{T}^*(\hat{z}(t)) \tag{7b}$$

where $\hat{z}(t)$ denotes the estimate of $z(t)$. Notice that KKL observer (7) is a special case of (2), where $\Phi(\hat{z}, y)$ is affine in $\hat{z}$ and $\Psi(\hat{z}, y) \coloneqq \mathcal{T}^*(\hat{z})$.

3.4 Existence Results

We explore sufficient conditions that ensure the existence of an injective transformation map $\mathcal{T}$ such that the estimate $\hat{x}(t)$ obtained from the KKL observer (7) satisfies the estimation error requirement (4).

Let the solution of (1a) initialized at $x_0 \in \mathcal{X}$ be $x(t; x_0)$.

Definition 1 *The system* (1) *is* forward complete *in $\mathcal{X}$ if, for every $x_0 \in \mathcal{X}$, the solution $x(t; x_0)$ exists for every $t \in \mathbb{R}_{\geq 0}$ and remains inside $\mathcal{X}$.*

Assumption 2 *There exists a compact set $\mathcal{X} \subset \mathbb{R}^{n_x}$ such that the system* (1) *is forward complete in $\mathcal{X}$.*

This assumption restricts our attention to nonlinear systems whose state $x(t)$ remains in a bounded domain.

Definition 3 *A map $\mathcal{T} : \mathcal{X} \to \mathcal{Z}$ is said to be* uniformly injective *if there exists a class $\mathcal{K}$ function*[3] *$\rho : \mathbb{R}_{\geq 0} \to \mathbb{R}_{\geq 0}$ such that, for every $x, \hat{x} \in \mathcal{X}$,*

$$\|x - \hat{x}\| \leq \rho(\|\mathcal{T}(x) - \mathcal{T}(\hat{x})\|). \tag{8}$$

Notice that (8) implies the existence of a class $\mathcal{K}$ function ϱ such that, for every $z, \hat{z} \in \mathcal{Z}$,

$$\|z - \hat{z}\| \leq \varrho(\|\mathcal{T}^*(z) - \mathcal{T}^*(\hat{z})\|). \tag{9}$$

Remark 4 *For the existence of a KKL observer* (7) *satisfying the requirement* (4)*, it is sufficient that* (1) *is forward complete and the map $\mathcal{T}$ satisfying the PDE* (6) *is uniformly injective; see [4, Theorem 1].* ◇

We have $\dot{\hat{z}}(t) - \dot{z}(t) = A[\hat{z}(t) - z(t)]$. Since A is chosen to be a Hurwitz matrix, $\|\hat{z}(t) - z(t)\|$ converges to zero exponentially. Thus, if $\mathcal{T}$ is uniformly injective, the estimation error $\xi(t)$ also converges to zero asymptotically because, from (8), we have

$$\|\xi(t)\| = \|x(t) - \hat{x}(t)\| \leq \rho(\|z(t) - \hat{z}(t)\|)$$

and $\rho(\|z(t) - \hat{z}(t)\|) \to 0$ as $\|z(t) - \hat{z}(t)\| \to 0$.

Definition 5 *Given an open set $\mathcal{O} \supset \mathcal{X}$, the system* (1) *is* backward $\mathcal{O}$-distinguishable *in $\mathcal{X}$ if, for every pair of distinct initial conditions $x_0^1, x_0^2 \in \mathcal{X}$, there exists $\tau \in \mathbb{R}_{<0}$ such that the backward solutions $x(t; x_0^1), x(t; x_0^2) \in \mathcal{O}$ exist for $t \in [\tau, 0]$, and*

$$h(x(\tau; x_0^1)) \neq h(x(\tau; x_0^2)).$$

[3] A function $\rho : \mathbb{R}_{\geq 0} \to \mathbb{R}_{\geq 0}$ is of class $\mathcal{K}$ if it is continuous, zero at zero, and strictly increasing. It is of class $\mathcal{K}_\infty$ if it is of class $\mathcal{K}$ and unbounded.

Although we assumed that (1) is forward complete in $\mathcal{X}$, it may not be backward complete in $\mathcal{X}$. That is, the state trajectories of (1) may leave $\mathcal{X}$, and may even go unbounded, in negative time ($t \in \mathbb{R}_{<0}$). The notion of backward $\mathcal{O}$-distinguishability guarantees the existence of a finite negative time such that the output maps, corresponding to a pair of trajectories initialized at different points in $\mathcal{X}$, can be distinguished before any of the trajectories leaves $\mathcal{O} \supset \mathcal{X}$ in backward time. Backward $\mathcal{O}$-distinguishability is related to the notions of determinability or constructability in linear systems [5, 11].

Assumption 6 *There exists an open bounded set $\mathcal{O} \supset \mathcal{X}$ such that* (1) *is backward $\mathcal{O}$-distinguishable in $\mathcal{X}$.*

It turns out that Assumptions 2 and 6 are sufficient for the existence of a *uniformly injective* map $\mathcal{T}$ satisfying (6). This result is obtained in slightly different forms in [4] and [11]. The most recent result provided by [14] can be restated as follows.

Theorem 7 *(Brivadis et al. [14]). Let Assumptions 2 and 6 hold. Then, for almost any $(A, B) \in \mathbb{R}^{n_z \times n_z} \times \mathbb{R}^{n_z \times n_y}$ such that*

(i) $n_z = n_y(2n_x + 1)$
(ii) A *is Hurwitz*
(iii) (A, B) *is controllable*

there exists a uniformly injective map $\mathcal{T} : \mathcal{X} \to \mathcal{Z}$ that satisfies the PDE (6)*.*

This theorem guarantees the existence of a uniformly injective map $\mathcal{T}$ and its left-inverse $\mathcal{T}^*$ such that the estimate $\hat{x}(t)$ obtained from the KKL observer (7) asymptotically converges to the true state $x(t)$. Therefore, relying on Assumptions 2 and 6, and fixing $n_z = n_y(2n_x+1)$, $A \in \mathbb{R}^{n_z \times n_z}$ a Hurwitz matrix, and $B \in \mathbb{R}^{n_z \times n_y}$ such that (A, B) is controllable, we can learn the transformation map $\mathcal{T}$ and its left-inverse $\mathcal{T}^*$.

4 Preliminaries on Learning Theory

We revisit the standard framework of statistical learning theory, which is relevant to this paper.

4.1 Learning Problem

Consider a supervised learning problem where the goal is to learn a mapping $\hat{\mathcal{T}} : \mathcal{X} \to \mathcal{Z}$ from an input space $\mathcal{X}$ to an output space $\mathcal{Z}$. We assume an unknown, fixed probability distribution $\mathcal{D}$ over $\mathcal{X} \times \mathcal{Z}$. The quality of a prediction $\hat{\mathcal{T}}(x)$ for a true output z is measured by a loss function $L(\hat{\mathcal{T}}(x), z)$.

The goal is to find a function $\hat{\mathcal{T}}$ that minimizes the *true* risk

$$R(\hat{\mathcal{T}}) = \mathbb{E}_{(x,z)\sim\mathcal{D}}[L(\hat{\mathcal{T}}(x), z)]$$

which is the expected loss over the true distribution $\mathcal{D}$. The minimal possible risk is the Bayes risk, $R^* = \inf_{\hat{\mathcal{T}}} R(\hat{\mathcal{T}})$, where the infimum is over all measurable functions [7]. Since $\mathcal{D}$ is unknown, we learn from a finite training sample $S = \{(x_i, z_i)\}_{i=1}^N$ of N examples drawn independently and identically distributed (i.i.d.) from $\mathcal{D}$. A learning algorithm is supposed to minimize the empirical risk

$$\hat{R}_S(\hat{\mathcal{T}}) = \frac{1}{N}\sum_{i=1}^{N} L(\hat{\mathcal{T}}(x_i), z_i)$$

on this sample S.

4.2 Hypothesis Class and Error Decomposition

A learning algorithm searches for a solution within a predefined hypothesis class $\mathcal{H}$, which is a set of functions $\hat{\mathcal{T}} : \mathcal{X} \to \mathcal{Z}$. For example, $\mathcal{H}$ can be the set of all functions representable by a specific neural network architecture. The empirical risk minimizer is the hypothesis $\hat{\mathcal{T}}_S \in \mathcal{H}$ that minimizes the empirical risk, i.e.,

$$\hat{\mathcal{T}}_S = \arg\min_{\hat{\mathcal{T}} \in \mathcal{H}} \hat{R}_S(\hat{\mathcal{T}}).$$

The *excess risk* $R(\hat{\mathcal{T}}_S) - R^*$ of the learned hypothesis, where R^* is the Bayes risk, can be decomposed into two fundamental components: approximation error

$$\inf_{\hat{\mathcal{T}} \in \mathcal{H}} R(\hat{\mathcal{T}}) - R^*$$

and estimation error

$$R(\hat{\mathcal{T}}_S) - \inf_{\hat{\mathcal{T}} \in \mathcal{H}} R(\hat{\mathcal{T}}).$$

The approximation error is deterministic and measures how well the chosen class $\mathcal{H}$ can, in principle, approximate the true optimal (Bayes) predictor. It is independent of the data size N. On the other hand, the estimation error is random (it depends on the sample S) and measures the penalty for having only a finite sample of N data points instead of the true distribution $\mathcal{D}$. A central goal of learning theory is to bound the estimation error, which requires a measure of the richness (or complexity) of the hypothesis class $\mathcal{H}$, as defined in the following subsection.

4.3 Pseudo-Dimension and Generalization Bounds

For real-valued functions, such as those in regression or in our KKL observer learning problem, the VC-dimension [51] (used for binary classification) is extended to the pseudo-dimension [25, 43]. This concept is defined not on the hypothesis class $\mathcal{H}$ itself, but on the associated loss class $\mathcal{G} = \{(x, z) \mapsto L(\hat{\mathcal{T}}(x), z) : \hat{\mathcal{T}} \in \mathcal{H}\}$.

Definition 8 *(Shattering and Pseudo-dimension [38]). A set of d points $\{(x_i, z_i)\}_{i=1}^d$ is* shattered *by the loss class $\mathcal{G}$ if there exist thresholds $\tau_1, \ldots, \tau_d \in \mathbb{R}$ such that for all 2^d possible binary labelings $b \in \{-1, +1\}^d$, there exists $\mathcal{T} \in \mathcal{H}$ whose corresponding loss $g \in \mathcal{G}$ satisfies*

$$\forall i \in \{1, \ldots, d\}, \quad \operatorname{sign}(g(x_i, z_i) - \tau_i) = b_i.$$

The pseudo-dimension *of $\mathcal{G}$, denoted* $\operatorname{Pdim}(\mathcal{G})$*, is the size d of the largest set that can be shattered by $\mathcal{G}$.*

The pseudo-dimension provides a combinatorial measure of the complexity of $\mathcal{H}$ via its loss class $\mathcal{G}$. A finite pseudo-dimension d ensures that the estimation error will decrease as the sample size N increases. This is formalized in a generalization bound below.

Lemma 9 *(Generalization Bound for Bounded Regression [38, Theorem 11.8]). Let $\mathcal{G}$ be a loss class with pseudo-dimension $d = \operatorname{Pdim}(\mathcal{G}) < \infty$. Assume the loss L is bounded by a constant M. Then, for any $\delta > 0$, with probability at least $1 - \delta$ over the draw of an i.i.d. sample S of size N, it holds that for every $\hat{\mathcal{T}} \in \mathcal{H}$,*

$$R(\hat{\mathcal{T}}) \leq \hat{R}_S(\hat{\mathcal{T}}) + M\sqrt{\frac{2d\ln(eN/d)}{N}} + M\sqrt{\frac{\ln(1/\delta)}{2N}}.$$

This lemma provides an explicit, non-asymptotic bound on the estimation error. The complexity term

$$\mathcal{C}(\mathcal{H}, N, \delta) \triangleq M\sqrt{\frac{2d\ln(eN/d)}{N}} + M\sqrt{\frac{\ln(1/\delta)}{2N}}$$

depends on the hypothesis class $\mathcal{H}$ via d and the sample size N. For the learning procedure of KKL observers developed in this paper, we derive such explicit non-asymptotic error bounds.

5 Learning Method for KKL Observers

Designing KKL observers involves (a) finding the injective map $\mathcal{T} : \mathcal{X} \to \mathcal{Z}$ that satisfies PDE (6), so that the nonlinear system (1) admits a linear up to output injection representation (5), and (b) finding its left-inverse $\mathcal{T}^*$, so that a state estimate can be obtained in the original state coordinates. For finding $\mathcal{T}$, one must solve PDE (6), whose explicit solution derived in [4] is given by

$$\mathcal{T}(x) = \int_{-\infty}^{0} \exp(A\tau)Bh(\breve{x}(\tau; x))\mathrm{d}\tau \tag{10}$$

where $\breve{x}(\tau; x) \in \mathcal{X}$ is the backward solution trajectory initialized at $x \in \mathcal{X}$, for $\tau \in \mathbb{R}_{\leq 0}$, to the modified dynamics $\dot{\breve{x}}(\tau) = g(\breve{x}(\tau))$ with $g(\breve{x}(\tau)) = f(\breve{x}(\tau))$ if $\breve{x}(\tau) \in \mathcal{X}$ and $g(\breve{x}(\tau)) = 0$ otherwise.

However, computing (10) is not practically possible [11] due to the inaccessibility of the backward output map $h(\breve{x}(\tau; x))$ for $\tau < 0$ and the infeasibility of computing the integral (10) for every initial point $x \in \mathcal{X}$. Note that, even if $\mathcal{T}$ is known in some other form [4] than (10), finding the left-inverse $\mathcal{T}^*$ is difficult both analytically and numerically [3]. To overcome these challenges, we propose learning the maps $\mathcal{T}$ and $\mathcal{T}^*$.

5.1 Learning Problem

We introduce two expectation operators corresponding to the underlying data distributions. Let $\mathcal{D}_{\mathcal{X}}$ be the true data distribution over the compact state space $\mathcal{X}$. The first expectation operator is formally defined with respect to this measure as

$$\mathbb{E}_{x\sim\mathcal{D}_{\mathcal{X}}}[\cdot] = \int_{\mathcal{X}} (\cdot)\ \mathrm{d}\mathcal{D}_{\mathcal{X}}(x).$$

The injective map $\mathcal{T} : \mathcal{X} \to \mathcal{Z}$ induces a pushforward measure $\mu_{\mathcal{T}}$ on the observer space $\mathcal{Z}$, defined by $\mu_{\mathcal{T}}(Z) = \mathcal{D}_{\mathcal{X}}(\mathcal{T}^{-1}(Z))$ for any measurable set $Z \subset \mathcal{Z}$. The second expectation operator is defined with respect to this measure as

$$\mathbb{E}_{z\sim\mu_{\mathcal{T}}}[\cdot] = \int_{\mathcal{Z}} (\cdot)\ \mathrm{d}\mu_{\mathcal{T}}(z).$$

Now, we define the risk and error functions associated with the learning of a KKL observer.

Our goal is to find approximations $\hat{\mathcal{T}}_\theta \in \mathcal{H}_\theta$ and $\hat{\mathcal{T}}^*_\eta \in \mathcal{H}_\eta$ for $\mathcal{T}$ and $\mathcal{T}^*$, where $\mathcal{H}_\theta$ and $\mathcal{H}_\eta$ are the hypothesis classes (e.g., neural network architectures) for the forward and inverse maps. The learned forward map $\hat{\mathcal{T}}_\theta$ must satisfy two conditions: (i) it must map x to the correct $z = \mathcal{T}(x)$, and (ii) it must satisfy the governing PDE (6). The *forward map error* is given by

$$R_{\mathcal{T}}(\theta) = \mathbb{E}_{x\sim\mathcal{D}_{\mathcal{X}}}\left[\|\mathcal{T}(x) - \hat{\mathcal{T}}_\theta(x)\|^2\right] \tag{11}$$

[4] See [10] for some examples.

and the PDE error by $R_{\text{PDE}}(\theta) = \mathbb{E}_{x\sim\mathcal{D}_\mathcal{X}}\left[\|\mathcal{P}_\theta(x)\|^2\right]$ where $\mathcal{P}_\theta(x)$ is the PDE residual

$$\mathcal{P}_\theta(x) \coloneqq \frac{\partial \hat{\mathcal{T}}_\theta}{\partial x}(x) f(x) - A\hat{\mathcal{T}}_\theta(x) - Bh(x). \tag{12}$$

We combine these into the *physics-informed risk*

$$R_1(\theta) = R_\mathcal{T}(\theta) + \nu R_{\text{PDE}}(\theta) \tag{13}$$

where $\nu > 0$ is a hyperparameter.

The learned inverse map $\hat{\mathcal{T}}^*_\eta$ must approximate the true inverse $\mathcal{T}^*$ by minimizing the *inverse map error*

$$R_{\mathcal{T}^*}(\eta) = \mathbb{E}_{z\sim\mu_\mathcal{T}}\left[\|\mathcal{T}^*(z) - \hat{\mathcal{T}}^*_\eta(z)\|^2\right] \tag{14}$$

where $\mu_\mathcal{T}$ is the pushforward measure on the observer space $\mathcal{Z}$. Moreover, to learn the KKL observer, $\hat{\mathcal{T}}^*_\eta$ must also reconstruct the state x from the output of the learned forward map $\hat{\mathcal{T}}_\theta(x)$. That is, given a fixed, learned map $\hat{\mathcal{T}}_\theta$, the learned inverse $\hat{\mathcal{T}}^*_\eta$ must minimize the *reconstruction risk*

$$R_2(\eta \mid \theta) = \mathbb{E}_{x\sim\mathcal{D}_\mathcal{X}}\left[\|x - \hat{\mathcal{T}}^*_\eta(\hat{\mathcal{T}}_\theta(x))\|^2\right]. \tag{15}$$

Our goal is to find parameters θ and η that sequentially minimize $R_1(\theta)$ and $R_2(\eta \mid \theta)$, respectively. Since the true data distribution $\mathcal{D}_\mathcal{X}$ and the true maps $\mathcal{T}$ and $\mathcal{T}^*$ are unknown, we minimize empirical approximations of these risks using synthetically generated data.

5.2 Data Generation Procedure

Before defining empirical approximations of these risks, we describe a heuristic for generating synthetic data. Since the observer matrices A and B are assumed to be fixed and the system functions f and h to be known, it is possible to generate trajectories of x and z numerically. However, given $x_0 \in \mathcal{X}$, one cannot guess the initial condition $z(0) = \mathcal{T}(x_0)$ because $\mathcal{T}$ is unknown. Following [44], one could mitigate this because, for an arbitrary $z(0) = z_0$, the solution of (5) satisfies

$$\|z(t; z_0)\| \leq \|\exp(At)z_0\| + \int_0^t \|\exp(A(t-\tau))By(\tau)\|d\tau.$$

Since A is Hurwitz, $\|\exp(At)z_0\| \to 0$ exponentially fast, and the effect of the initial condition z_0 vanishes from $z(t; z_0)$ over time t. We have $\|\exp(At)z_0\| \leq \text{cond}(V)e^{\lambda_{\min}(A)t}\|z_0\|$, where $\lambda_{\min}(A)$ defined in Section 3.1, and V obtained from the eigendecomposition of $A = V\Lambda V^{-1}$, which is assumed to be diagonalizable. For any $\varepsilon > 0$, there exists time t_* such that $\|\exp(At)z_0\| \leq \varepsilon$, for all $t \geq t_*$, where $t_* \coloneqq t_*(\varepsilon, z_0) = \frac{1}{\lambda_{\min}(A)} \ln\left(\frac{\varepsilon}{\text{cond}(V)\|z_0\|}\right)$. Therefore,

$$\forall t \geq t_*, \quad \|z(t; z_0)\| \leq \varepsilon + \int_0^t \|\exp(A(t-\tau))By(\tau)\|d\tau.$$

As time progresses, the trajectory $z(t; z_0^i)$ becomes almost independent of the initial condition z_0. This observation leads to the following data generation procedure.

Initial condition sampling: We sample $p \in \mathbb{Z}_{>0}$ initial points $\left\{(x_0^i, z_0^i)\right\}_{i\in[p]}$ uniformly in $\mathcal{X} \times \mathcal{Z}$.

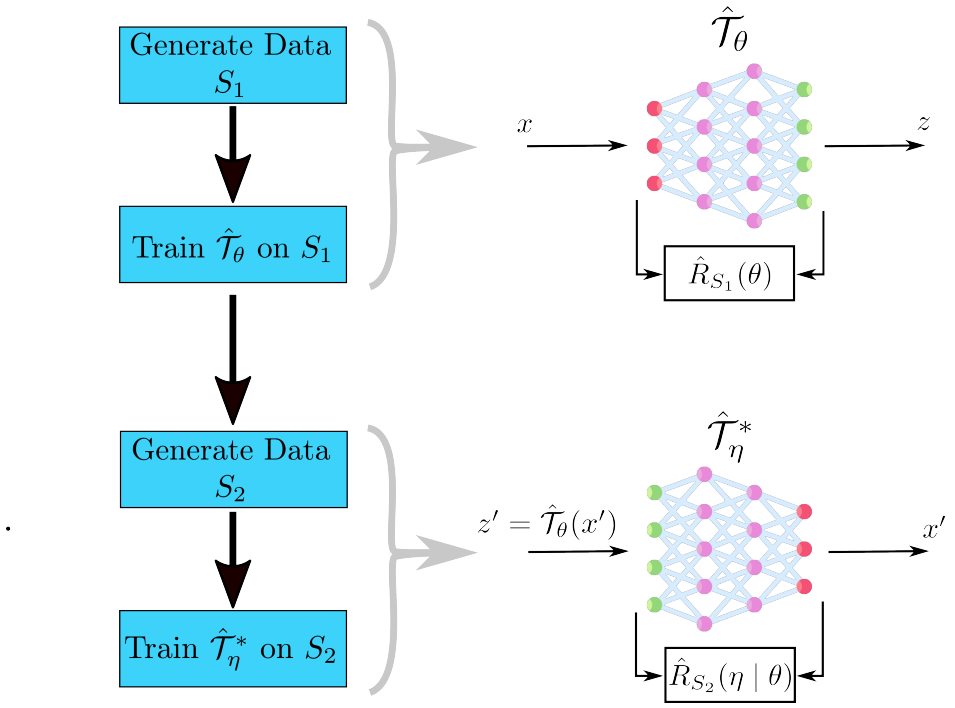

Fig. 1. Overview of the proposed KKL observer learning algorithm.

Trajectory generation: For all $i \in [p]$, we simulate (1) and (5) with initial condition (x_0^i, z_0^i) from $t_1 = 0$ to $t_\tau = T$, where $T \in \mathbb{R}_{>0}$ is chosen to be large.

Truncation: For all $i \in [p]$, the samples of the z-trajectory for $t_k \geq t_{k_*}$ are kept and the rest of the samples are discarded, where

$$k_* := \min \left\{ k \mid t_k \geq \max_{i \in [p]} t_*(\varepsilon, z_0^i) \right\}.$$

This procedure yields the training set

$$S_{\text{data}} = \{(x(t_k; x_0^i), z(t_k; z_0^i))\}_{i \in [p], k \in \{k_*, \dots, \tau\}}$$

containing truncated trajectories with $N_{\text{data}} = p(\tau - k_* + 1)$ data pairs. We further sample $q \in \mathbb{Z}_{>0}$ points x_0^j and generate trajectories

$$S_{\text{pde}} = \{x(t_k; x_0^j)\}_{j \in [q], k \in \{1, \dots, \tau\}}$$

with $N_{\text{pde}} = q\tau$ collocation points for the PDE. The data $S_1 = \{S_{\text{data}}, S_{\text{pde}}\}$ is used for learning the forward map $\hat{\mathcal{T}}_\theta$ with total number of data points $N_1 = N_{\text{data}} + N_{\text{pde}}$. After training the forward map $\hat{\mathcal{T}}_\theta$, its parameters θ are fixed. We then generate a new dataset $S_2 = \{(z'_j, x'_j)\}_{j=1}^{N_2}$ of size N_2, where x' are randomly sampled points in $\mathcal{X}$ or trajectories from randomly sampled initial points in $\mathcal{X}$, and the corresponding features $z'_j = \hat{\mathcal{T}}_\theta(x'_j)$ are generated from the learned forward map.

5.3 Empirical Risk Minimization

We approximate the true risks R_1 and R_2 in (13) and (15) with their empirical counterparts, computed from finite datasets S_1 and S_2. First, we minimize empirical physics-informed risk $\hat{R}_{S_1}$ using $S_1 = (S_{\text{data}}, S_{\text{pde}})$ with

$$\hat{R}_{S_1}(\theta) = \frac{1}{N_{\text{data}}} \sum_{(x,z)\in S_{\text{data}}} \|z - \hat{\mathcal{T}}_\theta(x)\|^2 + \frac{\nu}{N_{\text{pde}}} \sum_{x\in S_{\text{pde}}} \|\mathcal{P}_\theta(x)\|^2 \tag{16}$$

where $\mathcal{P}_\theta(x)$ is defined in (12). This risk is the computable objective function for the inverse map and approximates the true risk in (13). Thus, the first-stage empirical risk minimization problem is formulated as

$$\min_{\theta\in\mathcal{H}_\theta} \hat{R}_{S_1}(\theta). \tag{17}$$

We follow the sequential approach, first proposed by [41] for discrete-time systems. After training the forward map $\hat{\mathcal{T}}_\theta$, we generate a new dataset $S_2 = \{(z'_j, x'_j)\}_{j=1}^{N_2}$, where $z'_j = \hat{\mathcal{T}}_\theta(x'_j)$. On this dataset S_2, the empirical reconstruction risk is given by

$$\hat{R}_{S_2}(\eta \mid \theta) = \frac{1}{N_2} \sum_{j=1}^{N_2} \|x'_j - \hat{\mathcal{T}}^*_\eta(z'_j)\|^2 \tag{18}$$

which is the computable objective function for the inverse map and approximates the true risk in (15). Thus, the second-stage empirical risk minimization problem is formulated as

$$\min_{\eta\in\mathcal{H}_\eta} \hat{R}_{S_2}(\eta \mid \theta). \tag{19}$$

5.4 Remarks on the Learning Method

Fig. 1 illustrates the workflow of proposed learning algorithm. Our procedure deconstructs the autoencoder framework used in previous works, such as [39], into sequentially learning the maps $\hat{\mathcal{T}}_\theta$ and $\hat{\mathcal{T}}^*_\eta$. This idea serves to address two fundamental issues:

(1) The joint encoder decoder structure is inherently susceptible to conflicting gradients between components of the objective function, which might result in the optimization getting stuck in bad local minima. This not only degrades the accuracy of the learned solutions but also create the risk of failing to enforce the latent output of the autoencoder to reside within $\mathcal{Z}$, leading to a discrepancy between the input distributions of $\hat{\mathcal{T}}^*_\eta$ during online operation.

(2) The data generation process is dependent on the truncation of the simulated trajectories to get rid of the transient effects due to the initialization of z-trajectories using the contraction property of (5). However, this procedure does not allow us to freely choose pairings of initial conditions (x_0, z_0), which might result in uneven sampling of certain parts of the state space. This issue has previously been addressed in [15] and [39] by first simulating the system backward in time from the chosen initial conditions in $\mathcal{X}$, then obtaining the corresponding values in $\mathcal{Z}$ by simulating forward from negative time to $t = 0$. However, this setup is inherently infeasible for stable systems, and some unstable systems as well, that blow up in negative time.

In our sequential procedure, we first learn θ for the forward map $\hat{\mathcal{T}}_\theta : \mathcal{X} \to \mathcal{Z}$ by solving (17) on the dataset S_1. The learned forward map is then used to generate a new dataset S_2. The parameters η for the inverse map $\hat{\mathcal{T}}^*_\eta$ are

then learned by solving (19) on the new dataset S_2. Decoupling the training of $\hat{\mathcal{T}}_\theta$ and $\hat{\mathcal{T}}_\eta^*$ therefore avoids the risk of conflicting gradients between (16) and (18), while ensuring that $\hat{\mathcal{T}}_\theta$ and $\hat{\mathcal{T}}_\eta^*$ are indeed trained using data from correct distributions.

The formulation of the empirical physics-informed risk $\hat{R}_{S_1}(\theta)$ in (16) constitutes a semi-supervised learning framework. The data-fit term $\|z - \hat{\mathcal{T}}_\theta(x)\|^2$ is computed on the labeled data S_{data}. Conversely, the physics-informed risk term $\|\mathcal{P}_\theta(x)\|^2$ is evaluated on the unlabeled collocation data S_{pde}. This semi-supervised structure allows us to enforce the physical constraint (6) over a large, densely-sampled portion of the state space ($N_{\text{pde}} \gg N_{\text{data}}$), which acts as a powerful data-agnostic regularizer and prevents overfitting to the labeled S_{data}.

6 Non-Asymptotic Learning Guarantees

The learning method proposed in Section 5 computes the approximations $\hat{\mathcal{T}}_\theta$ and $\hat{\mathcal{T}}_\eta^*$. A critical question remains: does this learning procedure provide any guarantee that the resulting maps are "good" approximations of the true, unknown maps $\mathcal{T}$ and $\mathcal{T}^*$? The practical utility of the learned observer depends on this approximation quality. If the learned inverse map $\hat{\mathcal{T}}_\eta^*$ is a poor approximation of the true $\mathcal{T}^*$, the resulting estimate $\hat{x}(t) = \hat{\mathcal{T}}_\eta^*(\hat{z}(t))$ will be inaccurate, irrespective of the observer's dynamic properties.

This section provides theoretical guarantees for our learning-based design of KKL observers. We establish that the approximation error of the learning procedure is bounded. This error is quantified by the inverse map error $R_{\mathcal{T}^*}(\eta)$ defined in (14). Proving that $R_{\mathcal{T}^*}$ can be made small provides the foundation for our learning method.

6.1 Lipschitz Assumption

Given that the neural network's activation functions are Lipschitz continuous, the neural network map is also Lipschitz continuous. Thus, it is natural to make the following assumption.

Assumption 10 *The neural network $\hat{\mathcal{T}}_\eta^*$ is Lipschitz continuous over $\mathcal{Z}$, where $\mathcal{Z} \supseteq \mathcal{T}(\mathcal{X})$. In particular, for every $z, \hat{z} \in \mathcal{Z}$, there exists $\ell_\eta \in \mathbb{R}_{>0}$ such that*

$$\|\hat{\mathcal{T}}_\eta^*(z) - \hat{\mathcal{T}}_\eta^*(\hat{z})\| \leq \ell_\eta \|z - \hat{z}\|. \tag{20}$$

Estimating a neural network's Lipschitz constant is a topic of interest in the machine learning community [23, 26, 48, 52]. For feedforward ReLU networks, [20] shows that the local Lipschitz constant estimation problem can be reduced to a semidefinite program.

6.2 Generalization Guarantees

Recall that our learning method is a sequential procedure. First, we learn $\hat{\mathcal{T}}_\theta \in \mathcal{H}_\theta$ by minimizing the empirical physics-informed risk $\hat{R}_{S_1}(\theta)$. Then, we learn $\hat{\mathcal{T}}_\eta^* \in \mathcal{H}_\eta$ by minimizing the empirical reconstruction risk $\hat{R}_{S_2}(\eta \mid \theta)$. The inverse map error $R_{\mathcal{T}^*}$ is thus affected by the outcomes of both stages. In the following lemma, we relate $R_{\mathcal{T}^*}$ to the reconstruction risk $R_2(\eta \mid \theta)$ in (15), which is empirically minimized in the second stage, and the forward map error $R_{\mathcal{T}}(\theta)$ in (11), which is propagated from the first stage.

Lemma 11 *Let Assumption 10 hold. Then, the true inverse error $R_{\mathcal{T}^*}(\eta)$ in (14) is bounded by*

$$R_{\mathcal{T}^*}(\eta) \leq 2R_2(\eta \mid \theta) + 2\ell_\eta^2 R_{\mathcal{T}}(\theta) \tag{21}$$

where $R_2(\eta \mid \theta)$ is the reconstruction risk (15)*, $R_{\mathcal{T}}(\theta)$ is the forward map error* (11)*, and ℓ_η is the Lipschitz constant in* (20)*.*

PROOF. Let $\|\cdot\|_{L_2(\mathcal{D}_\mathcal{X})}$ denote the L_2 norm with respect to the data distribution $\mathcal{D}_\mathcal{X}$. Then,

$$\begin{aligned}\sqrt{R_{\mathcal{T}^*}} &= \|\mathcal{T}^*(\mathcal{T}) - \hat{\mathcal{T}}_\eta^*(\mathcal{T})\|_{L_2(\mathcal{D}_\mathcal{X})} \\ &\le \|\mathcal{T}^*(\mathcal{T}) - \hat{\mathcal{T}}_\eta^*(\hat{\mathcal{T}}_\theta)\|_{L_2(\mathcal{D}_\mathcal{X})} \\ &\qquad + \|\hat{\mathcal{T}}_\eta^*(\hat{\mathcal{T}}_\theta) - \hat{\mathcal{T}}_\eta^*(\mathcal{T})\|_{L_2(\mathcal{D}_\mathcal{X})} \\ &\le \sqrt{R_2(\eta \mid \theta)} + \ell_\eta \|(\hat{\mathcal{T}}_\theta - \mathcal{T})\|_{L_2(\mathcal{D}_\mathcal{X})} \\ &= \sqrt{R_2(\eta \mid \theta)} + \ell_\eta \sqrt{R_\mathcal{T}}\end{aligned}$$

where we used $x = \mathcal{T}^*(\mathcal{T}(x))$, the triangle inequality, Assumption 10, and definitions (15) and (11). Squaring both sides using the inequality $(a+b)^2 \le 2a^2 + 2b^2$ gives the desired result (21). □

Lemma 11 states that the inverse map error $R_{\mathcal{T}^*}$ is bounded by the reconstruction risk $R_2(\eta \mid \theta)$ and the forward error $R_\mathcal{T}$, which is amplified by the Lipschitz constant of the learned inverse map. We now bound these two terms using the generalization bound presented in Section 4.

Lemma 12 *Let $\mathcal{H}_\eta$ be the hypothesis class for the learned inverse map $\hat{\mathcal{T}}_\eta^*$. Let $\mathcal{G}_\eta = \{(x', z') \mapsto \|x' - \hat{\mathcal{T}}_\eta^*(z')\|^2 : \hat{\mathcal{T}}_\eta^* \in \mathcal{H}_\eta\}$ be the associated loss class, with finite pseudo-dimension $d_\eta = \mathrm{Pdim}(\mathcal{G}_\eta)$, where $z' = \hat{\mathcal{T}}_\theta(x)$. Let N_2 be the number of data points in the dataset $S_2 = \{(x'_j, z'_j)\}$. Assume the empirical reconstruction risk $\hat{R}_{S_2}(\eta \mid \theta)$ is bounded by M_η. Then, for any $\delta > 0$, with probability at least $1 - \delta$, we have*

$$R_2(\eta \mid \theta) \le \inf_{\hat{\eta} \in \mathcal{H}_\eta} \hat{R}_{S_2}(\hat{\eta} \mid \theta) + 2\mathcal{C}_\eta(N_2, \mathcal{H}_\eta, \delta) \tag{22}$$

where $\mathcal{C}_\eta(N_2, \mathcal{H}_\eta, \delta) = M_\eta \sqrt{\frac{2d_\eta \ln(eN_2/d_\eta)}{N_2}} + M_\eta \sqrt{\frac{\ln(1/\delta)}{2N_2}}$, R_2 defined in (15)*, and $\hat{R}_{S_2}$ in* (18)*.*

Lemma 13 *Let $\mathcal{H}_\theta$ be the hypothesis class for the learned forward map $\hat{\mathcal{T}}_\theta$. Let $\mathcal{G}_\theta$ be the associated loss class for the empirical physics-informed risk $\hat{R}_{S_1}(\theta)$ in* (16)*, with finite pseudo-dimension $d_\theta = \mathrm{Pdim}(\mathcal{G}_\theta)$. Let N_1 be the number of data points in S_1. Assume $\hat{R}_{S_1}(\theta) \le M_\theta$. Then, for any $\delta > 0$, with probability at least $1 - \delta$,*

$$R_1(\theta) \le \inf_{\theta \in \mathcal{H}_{\hat{\theta}}} \hat{R}_{S_1}(\hat{\theta}) + 2\mathcal{C}_\theta(N_1, \mathcal{H}_\theta, \delta) \tag{23}$$

where $\mathcal{C}_\theta(N_1, \mathcal{H}_\theta, \delta) = M_\theta \sqrt{\frac{2d_\theta \ln(eN_1/d_\theta)}{N_1}} + M_\theta \sqrt{\frac{\ln(1/\delta)}{2N_1}}$, R_1 defined in (13)*, and $\hat{R}_{S_1}$ in* (16)*.*

Moreover, since $R_\mathcal{T}(\theta) \le R_1(\theta)$, the right-hand side of (23) *also provides a high-probability bound on $R_\mathcal{T}$.*

Lemmas 12 and 13 are direct applications of the generalization bound in Lemma 9 to the empirical risk minimization problems (19) and (17). In these lemmas, the assumptions that the empirical risks are bounded by constants M_η and M_θ are justified by the compactness of the state space $\mathcal{X}$ (Assumption 2). Since the neural networks $\hat{\mathcal{T}}_\theta, \hat{\mathcal{T}}_\eta^*$ utilize continuous activation functions and the system maps f, h and the transformation $\mathcal{T}$ are continuous, the empirical risk functions, which are composed of squared errors and PDE residuals, are continuous functions defined on a compact set. Therefore, by the Extreme Value Theorem, they strictly admit finite upper bounds.

6.3 Main Theorem and Discussion

We provide a high-probability bound on the true L_2 approximation error $R_{\mathcal{T}^*}$ of the learned inverse map $\hat{\mathcal{T}}_\eta^*$ by combining the results of the above lemmas.

Theorem 14 *Let $\hat{\mathcal{T}}_\theta \in \mathcal{H}_\theta$ and $\hat{\mathcal{T}}_\eta^* \in \mathcal{H}_\eta$ be the maps learned by the proposed learning method. Let Assumption 10 hold. Then, for any $\delta > 0$, with probability at least $1 - 2\delta$, it holds that*

$$R_{\mathcal{T}^*}(\eta) \leq 2\left(\hat{R}_2(\eta \mid \theta) + 2\mathcal{C}_\eta(N_2, \mathcal{H}_\eta, \delta)\right) + 2\ell_\eta^2\left(\hat{R}_1(\theta) + 2\mathcal{C}_\theta(N_1, \mathcal{H}_\theta, \delta)\right) \tag{24}$$

where $R_{\mathcal{T}^*}(\eta)$ is the inverse map error in (14), $\hat{R}_2(\eta) = \inf_{\hat{\eta}\in\mathcal{H}_\eta} \hat{R}_{S_2}(\eta \mid \theta)$ is the approximation error of the inverse map, $\hat{R}_1 = \inf_{\hat{\theta}\in\mathcal{H}_\theta} \hat{R}_{S_1}(\theta)$ is the approximation error of the forward map, and $\mathcal{C}_\eta$ and $\mathcal{C}_\theta$ are the explicit complexity terms defined in Lemmas 12 and 13, which vanish as the data sizes N_2 and N_1 tend to infinity.

The proof follows from Lemmas 11, 12, and 13. Below, we discuss some implications of the theorem and present guidelines for the learning algorithm.

Theorem 14 provides an explicit, non-asymptotic bound on the inverse map error $R_{\mathcal{T}^*}$. It provides a theoretical guarantee for the learning algorithm presented in Section 5. It demonstrates that $R_{\mathcal{T}^*}$ can be made small, provided the empirical approximation errors, $\hat{R}_2$ and $\hat{R}_{S_1}$, and the estimation errors, $\mathcal{C}_\theta$ and $\mathcal{C}_\eta$, are small. This is achieved by using sufficiently rich network architectures $\mathcal{H}_\theta$ and $\mathcal{H}_\eta$ (e.g., deep and wide) to be able to represent the true maps $\mathcal{T}$ and $\mathcal{T}^*$, leveraging the universal approximation property of neural networks. Moreover, the estimation error terms $\mathcal{C}_\eta$ and $\mathcal{C}_\theta$ decrease as the data sizes N_1 and N_2 increase. This justifies the data-generation procedure and shows that a larger dataset results in a lower inverse map error.

The bound (24) also depends on the forward map error $R_{\mathcal{T}}$, which represents the error from learning the forward map $\hat{\mathcal{T}}_\theta$ and can be bounded as $R_{\mathcal{T}} \leq R_1 \leq \hat{R}_1 + 2\mathcal{C}_\theta$ (Lemma 13). However, this error $R_{\mathcal{T}}$ is amplified by ℓ_η^2 in (24). Since the Lipschitz constant ℓ_η depends on the norm of the neural network weights, regularizing the weights of the inverse map $\hat{\mathcal{T}}_\eta^*$ results in a smaller ℓ_η.

The role of our physics-informed learning method is as follows. The bound (24) on $R_{\mathcal{T}^*}$ depends on $R_{\mathcal{T}}$, which is bounded by R_1. Therefore, minimizing the PDE residual $\|\mathcal{P}_\theta\|^2$ (the physics-informed component of $\hat{R}_{S_1}(\theta)$ in (16)) is not just a heuristic; it is essential for provably reducing the forward map error $R_{\mathcal{T}}$ and, consequently, for minimizing the inverse map error $R_{\mathcal{T}^*}$. The guarantee that we can learn an accurate inverse map $\hat{\mathcal{T}}_\eta^*$ is the fundamental prerequisite for analyzing the observer's performance in the presence of noise and uncertainties, which we will show in the next section.

Additionally, the physics-informed risk component ($\hat{R}_1$ and $\mathcal{C}_\theta$) in the bound (24) highlights the theoretical benefit of our approach. A standard supervised method (i.e., with $\nu = 0$) would search for a minimizer within the entire, unconstrained hypothesis class $\mathcal{H}_\theta$. In contrast, incorporating the PDE constraint acts as a powerful inductive bias. It implicitly restricts the optimization to an effective hypothesis space, $\mathcal{H}_{\theta,\text{PDE}} \subset \mathcal{H}_\theta$, which contains only those functions that are physically plausible (i.e., that nearly satisfy the KKL PDE (6)). This effective space is significantly less complex than $\mathcal{H}_\theta$, implying that its pseudo-dimension $d_{\theta,\text{PDE}}$ is much smaller than the pseudo-dimension d_θ of the unconstrained class. Consequently, the complexity term $\mathcal{C}_\theta$ (defined in Lemma 13) is substantially reduced. This demonstrates that the physics-informed approach not only finds a more accurate solution (lower $\hat{R}_1$) but also achieves a better generalization guarantee (lower estimation error) from a finite dataset S_1.

7 Robustness of Learned KKL Observer

The neural networks $\hat{\mathcal{T}}_\theta$ and $\hat{\mathcal{T}}^*_\eta$ aproximate $\mathcal{T}$ and $\mathcal{T}^*$, respectively. Approximation errors affect the observer's estimation performance when we use neural networks instead of the original transformation maps. For any $z \in \mathcal{Z}$, the true inverse $\mathcal{T}^*(z)$ can be written as

$$\mathcal{T}^*(z) = \hat{\mathcal{T}}^*_\eta(z) + \mathcal{E}^*_\eta(z) \tag{25}$$

where $\mathcal{E}^*_\eta$ denotes the approximation error of the learned inverse map $\hat{\mathcal{T}}^*_\eta$. The learned KKL observer is given by

$$\begin{aligned} \dot{\hat{z}}(t) &= A\hat{z}(t) + By(t), \quad \hat{z}(0) = \hat{z}_0 \\ \hat{x}(t) &= \hat{\mathcal{T}}^*_\eta(\hat{z}(t)). \end{aligned} \tag{26}$$

The estimate obtained by this observer is affected by the approximation error $\mathcal{E}^*_\eta(\hat{z}(t))$, which acts as an unknown noise. Additionally, the system model (1) is rarely perfect in practice, and underlying uncertainties can affect the estimation performance. In this section, we provide robustness guarantees for the estimation error under both approximation error and system uncertainties.

7.1 Problem Setup and Assumptions

Consider an uncertain nonlinear system

$$\dot{x}(t) = f(x(t)) + w(t), \quad x(0) = x_0 \tag{27a}$$
$$y(t) = h(x(t)) + v(t) \tag{27b}$$

where $w(t) \in \mathbb{R}^{n_x}$ and $v(t) \in \mathbb{R}^{n_y}$ denote the model uncertainty and the measurement noise, respectively. For uncertain systems, the objective of the observer changes from steering the estimation error to zero as in (4) to steering it "close" to zero. That is, the observer must ensure that the estimation error (3) satisfies an input-to-state stability bound

$$\|\xi(t)\| \leq \beta(\|\xi_0\|, t) + \gamma_1(\|w_{[0,t]}\|_{L_\infty}) + \gamma_2(\|v_{[0,t]}\|_{L_\infty}) \tag{28}$$

where $\xi(t)$ is the estimation error defined in (3), $\xi_0 = \xi(0)$ is the initial estimation error, β is a class-$\mathcal{KL}$ function [5] that asymptotically converges to zero as $t \to \infty$, and γ_1, γ_2 are class-$\mathcal{K}_\infty$ functions. From (28), it is evident that in the absence of uncertainty $w(t)$ and noise $v(t)$, the estimate $\hat{x}(t)$ asymptotically converges to the true state $x(t)$, thus satisfying (4). Moreover, (28) imposes a robustness criterion on the observer's state estimate under uncertainties. In other words, as the magnitudes of the uncertainties increase, (28) ensures that there is a graceful degradation of the state estimate, so the estimation error remains bounded as long as the uncertainties are bounded.

Let $x(t; x_0, w)$ denote the state of (27a) at time $t \in \mathbb{R}_{\geq 0}$ initialized at $x(0) = x_0$ and driven by uncertainty $w_{[0,t]}$. When $w \equiv 0$, the state trajectory is denoted by $x(t; x_0)$.

Assumption 15 *The model uncertainty $w(t)$ and the measurement noise $v(t)$ satisfy the following:*

(i) Boundedness: It holds that $\|w\|_{L_\infty} < \overline{w}$ and $\|v\|_{L_\infty} < \overline{v}$, for some known $\overline{w}, \overline{v} > 0$.
(ii) Bounded effect of w: There exists a class $\mathcal{K}_\infty$ function ψ such that, for every $t \in \mathbb{R}_{\geq 0}$,

$$\|x(t; x_0, w) - x(t; x_0)\| \leq \psi(\|w_{[0,t]}\|_{L_\infty}).$$

[5] A function $\beta : \mathbb{R}_{\geq 0} \times \mathbb{R}_{\geq 0} \to \mathbb{R}_{\geq 0}$ is of class $\mathcal{KL}$ if (i) for each fixed $t \in \mathbb{R}_{\geq 0}$, $\beta(r, t)$ is of class $\mathcal{K}$, and (ii) for each fixed $r \in \mathbb{R}_{\geq 0}$, $\beta(r, t)$ is decreasing in t and is such that $\beta(r, t) \to 0$ as $t \to \infty$.

Assumption 15(i) is quite standard in robust state estimation [17]. Assumption 15(ii) requires that the deterministic system (1) does a good job in describing the uncertain system (27). Providing such a guarantee is widely studied in system identification, and the reader is referred to [1, 31, 35, 37] for more details.

Define the error in the z-coordinate as $\tilde{z}(t) \coloneqq z(t) - \hat{z}(t)$. Then, from (5) and (26), we have

$$\dot{\tilde{z}}(t) = A\tilde{z}(t) + B\sigma(t) \tag{29}$$

where $\sigma(t) = h(\bar{x}(t)) - h(x(t)) - v(t)$ with $x(t) \coloneqq x(t; x_0, w)$ and $\bar{x}(t) \coloneqq x(t; x_0)$. Note that $\sigma(t) \in \mathbb{R}^{n_y}$ remains bounded due to Assumption 15. That is, for every $x(t), \bar{x}(t) \in \mathcal{X}$ and $t \in \mathbb{R}_{\geq 0}$,

$$\begin{aligned}
\|\sigma(t)\| &\leq \|h(\bar{x}(t)) - h(x(t))\| + \|v(t)\| \\
&\leq \ell_h \|\bar{x}(t) - x(t)\| + \|v(t)\| \\
&\leq \ell_h \psi(\|w_{[0,t]}\|_{L_\infty}) + \|v(t)\| \\
&\leq \ell_h \psi(\overline{w}) + \sqrt{n_y}\overline{v}
\end{aligned} \tag{30}$$

where $\overline{w}, \overline{v}$ are from Assumption 15(i) and $\ell_h < \infty$ with

$$\ell_h = \sup_{x \in \mathcal{X}} \sigma_{\max}\left(\frac{\partial h}{\partial x}(x)\right) \tag{31}$$

because $h(\cdot)$ is smooth and $\mathcal{X}$ is a compact set. In the last step of (30), we used

$$\|v(t)\| \leq \sqrt{n_y}\|v(t)\|_\infty \leq \sqrt{n_y}\|v_{[0,t]}\|_{L_\infty} \leq \sqrt{n_y}\overline{v}.$$

7.2 Technical Lemmas

The lemmas below are needed in proving the theorems later in this section. Recall $z = \mathcal{T}(x)$, where $\dot{z}(t) = Az(t) + Bh(\bar{x}(t))$ with $\bar{x}(t) \coloneqq x(t; x_0)$ the noise-free state trajectory. Also, recall the dynamics of $\hat{z}(t) = \hat{\mathcal{T}}_\theta(\hat{x}(t))$ given in (26).

Lemma 16 *Suppose A is Hurwitz and diagonalizable with eigenvalue decomposition $A = V\Lambda V^{-1}$. Then,*

$$\|\exp(At)\| \leq \operatorname{cond}(V) e^{\lambda_{\min}(A)t}$$

and

$$\int_0^t \|\exp(A\tau)B\| d\tau \leq \frac{\operatorname{cond}(V)}{|\lambda_{\min}(A)|}\|B\|(1 - e^{\lambda_{\min}(A)t}).$$

A similar result can be obtained when A is not diagonalizable by using the Jordan form of A; see [47, Appendix C.5]. However, since diagonalizable matrices are dense in the space of square matrices and also since A is a design matrix, the diagonalizability assumption is mild.

Lemma 17 *Let Assumption 15 hold. Then, the error $\tilde{z}(t) \coloneqq z(t) - \hat{z}(t)$ in the z-coordinate satisfies*

$$\|\tilde{z}(t)\| \leq \|\tilde{z}_0\| \operatorname{cond}(V) e^{\lambda_{\min}(A)t} + \frac{\operatorname{cond}(V)}{|\lambda_{\min}(A)|} \|B\| (1 - e^{\lambda_{\min}(A)t}) \big[\ell_h \psi(\overline{w}) + \sqrt{n_y}\overline{v}\big] \tag{32}$$

where $\overline{w}, \overline{v}, \psi$ are given in Assumption 15, and ℓ_h is the Lipschitz constant of $h(x)$ for $x \in \mathcal{X}$ given in (31)*.*

PROOF. Recall $\sigma(t) = h(\bar{x}(t)) - h(x(t)) - v(t)$ from (29). Then, the solution $\tilde{z}(t; \tilde{z}_0, \sigma)$ of (29) satisfies

$$\|\tilde{z}(t)\| \leq \|\exp(At)\tilde{z}_0\| + \int_0^t \|\exp(A\tau)B\sigma(t-\tau)\| \mathrm{d}\tau. \tag{33}$$

The second term on the right-hand side of (33) satisfies

$$\begin{aligned} &\int_0^t \|\exp(A\tau)B\sigma(t-\tau)\| \mathrm{d}\tau \\ &\qquad \leq \int_0^t \|\exp(A\tau)B\| \|\sigma(t-\tau)\| \mathrm{d}\tau \\ &\qquad \leq \int_0^t \|\exp(A\tau)B\| \mathrm{d}\tau \max_{\tau \geq 0} \|\sigma(\tau)\|. \end{aligned} \tag{34}$$

From (30), it follows that $\max_{\tau \geq 0} \|\sigma(\tau)\| \leq \ell_h \psi(\overline{w}) + \sqrt{n_y}\overline{v}$. Substituting this in (34) and in (33), and using Lemma 16, we obtain (32). □

7.3 Robustness to the Approximation Error

To analyze the observer's performance, we employ some measure-theoretic concepts. Recall the general probability measure $\mathcal{D}_{\mathcal{X}}$ over the compact state space $\mathcal{X}$. To describe the asymptotic, long-term statistical distribution of the system's trajectories, we consider physical invariant measures [21, 53]. For the autonomous nonlinear system (1), μ is a physical invariant measure if the probability of the state being in any set $X \subseteq \mathcal{X}$ remains constant under the system's flow [6]. Note that in deterministic dynamical systems, the state evolution itself is not random. However, the randomness originates from the system initialization. Therefore, any probabilistic statement refers to an ensemble of trajectories generated by a distribution of initial conditions.

The primary objective of the observer is to minimize estimation error under the system's long-term, steady-state operating conditions. For many nonlinear systems, especially the ones we consider in Section 8, the asymptotic behavior is confined to the attractor, whose statistics are governed by the invariant measure μ. The generalization bounds derived in Theorem 14 guarantee that the inverse map error $R_{\mathcal{T}^*}(\eta)$ is small only if the distribution $\mathcal{D}_{\mathcal{X}}$ is consistent with the distribution encountered during future operation. If $\mathcal{D}_{\mathcal{X}}$ instead would be some transient initial distribution, minimizing the generalization error would not guarantee accuracy at steady state. In this section, by setting $\mathcal{D}_{\mathcal{X}} = \mu$, we ensure the domain over which we proved the learning guarantee (Theorem 14) is the same domain over which we guarantee stability of the estimation error.

Given the invariant measure μ, the injective KKL transformation map $\mathcal{T} : \mathcal{X} \to \mathcal{Z}$ induces a pushforward measure $\mu_{\mathcal{T}}$ on the observer space $\mathcal{Z}$, defined by $\mu_{\mathcal{T}}(Z) = \mu(\mathcal{T}^{-1}(Z))$, $\forall Z \subseteq \mathcal{Z}$. Because μ is the invariant measure, the induced measure $\mu_{\mathcal{T}}$ represents the steady-state distribution of the transformed states z. The expectation $\mathbb{E}_{z \sim \mu_{\mathcal{T}}}[\cdot]$ with

respect to this measure is the formal definition of the steady-state expectation because, for any function $g : \mathcal{Z} \to \mathbb{R}$,

$$\mathbb{E}_{z\sim\mu_{\mathcal{T}}}[g(z)] = \int_{\mathcal{Z}} g(z)\mathrm{d}\mu_{\mathcal{T}}(z) = \int_{\mathcal{X}} g(\mathcal{T}(x))\mathrm{d}\mu(x) = \mathbb{E}_{x\sim\mu}[g(\mathcal{T}(x))].$$

Since the estimate $\hat{x}(t)$ is obtained from the learned observer (26), we have $x(t) - \hat{x}(t) = \mathcal{T}^*(z(t)) - \hat{\mathcal{T}}^*_\eta(\hat{z}(t))$. Thus, the steady-state estimation error is given by

$$\xi_{ss}(\zeta) \coloneqq \lim_{t\to\infty} \left[\mathcal{T}^*(z(t)) - \hat{\mathcal{T}}^*_\eta(\hat{z}(t))\right] \tag{35}$$

where $\zeta = \lim_{t\to\infty} z(t)$. The high-probability bound on the inverse map error $R_{\mathcal{T}^*}$ in Theorem 14 shows that our learning procedure can find an inverse map $\hat{\mathcal{T}}^*_\eta$ that is, on average, close to the true inverse $\mathcal{T}^*$. We now analyze the consequence of this approximation by demonstrating how $R_{\mathcal{T}^*}$ directly governs the steady-state performance and robustness of the learned observer (26). We first analyze the noise-free case and then extend the result to uncertain systems.

Theorem 18 *Let Assumptions 2, 6, and 10 hold. Let $\hat{x}(t)$ be the state estimate from the learned KKL observer* (26) *for the noise-free system* (1)*. Then, the expected squared steady-state estimation error is bounded as follows*

$$\mathbb{E}_{\zeta\sim\mu_{\mathcal{T}}}\left[\|\xi_{ss}(\zeta)\|^2\right] \le 2R_{\mathcal{T}^*}$$

where $\xi_{ss}(\zeta)$ is the steady-state error given in (35) *and $R_{\mathcal{T}^*}$ is the inverse map error* (14) *bounded by* (24)*.*

PROOF. From (25) and (29), the estimation error $\xi(t) = x(t) - \hat{x}(t)$ satisfies

$$\begin{aligned}\|\xi(t)\| &= \|\mathcal{T}^*(z(t)) - \hat{\mathcal{T}}^*_\eta(\hat{z}(t))\| \\ &\le \|\hat{\mathcal{T}}^*_\eta(z(t)) - \hat{\mathcal{T}}^*_\eta(\hat{z}(t))\| + \|\mathcal{T}^*(z(t)) - \hat{\mathcal{T}}^*_\eta(z(t))\| \\ &\le \ell_\eta\|\tilde{z}(t)\| + \|\mathcal{E}^*_\eta(z(t))\|\end{aligned}$$

where $\tilde{z}(t) = \hat{z}(t) - z(t)$ and $\mathcal{E}^*_\eta(z(t))$ given by (25). Using the inequality $(a+b)^2 \le 2a^2 + 2b^2$, we have

$$\|\xi(t)\|^2 \le 2\ell_\eta^2\|\tilde{z}(t)\|^2 + 2\|\mathcal{E}^*_\eta(z(t))\|^2.$$

Since A is Hurwitz, $\tilde{z}(t)$ converges to zero exponentially. Therefore, $2\ell_\eta^2\|\tilde{z}(t)\|^2$ vanishes as $t \to \infty$. By taking the limit on both sides and $\zeta = \lim_{t\to\infty} z(t)$, we obtain

$$\|\xi_{ss}(\zeta)\|^2 \le 2\|\mathcal{E}^*_\eta(\zeta)\|^2.$$

We now take the expectation of this inequality over the steady-state invariant measure $\mu_{\mathcal{T}}$, which gives

$$\mathbb{E}_{\zeta\sim\mu_{\mathcal{T}}}[\|\xi_{ss}(\zeta)\|^2] \le 2\mathbb{E}_{\zeta\sim\mu_{\mathcal{T}}}[\|\mathcal{E}^*_\eta(\zeta)\|^2] = 2R_{\mathcal{T}^*}.$$

This concludes the proof. □

This theorem provides a link between the learning guarantee in Theorem 14 and the observer's long-term performance. It shows that the expected steady-state estimation error is directly bounded by the inverse map error $R_{\mathcal{T}^*}$. This result is highly practical as Theorem 14 gives a recipe for reducing $R_{\mathcal{T}^*}$ (i.e., more data, appropriate network complexity, ℓ_η regularization), whereas Theorem 18 proves that doing so provably improves the average-case performance of the KKL observer's state estimate.

7.4 Robustness to Uncertainty and Noise

We now analyze the robustness of the learned observer (26) to estimate the state of an uncertain nonlinear system (27). Note that the design method of KKL observers as presented in Sections 3 and 5 remains the same for (27).

Theorem 19 *Let Assumptions 2, 6, 10, and 15 hold. Let $\hat{x}(t) = \hat{\mathcal{T}}_\eta^*(\hat{z}(t))$ be the estimate from (26) for the uncertain system (27). Suppose A is diagonalizable with eigendecomposition $A = V\Lambda V^{-1}$. Then, the expected squared steady-state estimation error satisfies*

$$\mathbb{E}_{\zeta\sim\mu_\mathcal{T}}\left[\|\xi_{ss}(\zeta)\|^2\right] \leq 2R_{\mathcal{T}^*} + 2\ell_\eta^2 \left(\frac{\operatorname{cond}(V)}{|\lambda_{\min}(A)|}\|B\|\right)^2 \left(\ell_h\psi(\overline{w}) + \sqrt{n_y}\overline{v}\right)^2 \tag{36}$$

where ξ_{ss} is given in (35), $R_{\mathcal{T}^*}$ is bounded by (24), $\overline{w}, \overline{v}, \psi$ are given in Assumption 15, ℓ_h is given in (31), ℓ_η is given in (20), and n_y is the dimension of the output vector $y(t)$.

PROOF. We begin from the same squared inequality as in the proof of Theorem 18, given by

$$\|\xi(t)\|^2 \leq 2l_\eta^2\|\tilde{z}(t)\|^2 + 2\|\mathcal{E}_\eta^*(z(t))\|^2.$$

We use Lemma 17 to bound $\|\tilde{z}(t)\|$. As $t \to \infty$, the exponential transient term decays to zero, leaving the steady-state bound

$$\limsup_{t\to\infty}\|\tilde{z}(t)\| \leq \frac{\operatorname{cond}(V)}{|\lambda_{\min}(A)|}\|B\|[\ell_h\psi(\overline{w}) + \sqrt{n_y}\overline{v}].$$

Let $C_z = \frac{\operatorname{cond}(V)}{|\lambda_{\min}(A)|}\|B\|[l_h\psi(\overline{w}) + \sqrt{n_y}\overline{v}]$. Then, the steady-state estimation error is bounded by

$$\limsup_{t\to\infty}\|\xi(t)\|^2 \leq 2l_\eta^2 C_z^2 + \limsup_{t\to\infty} 2\|\mathcal{E}_\eta^*(z(t))\|^2.$$

Taking the expectation over the steady-state invariant measure yields

$$\mathbb{E}_{\zeta\sim\mu_\mathcal{T}}[\|\xi_{ss}(\zeta)\|^2] \leq 2l_\eta^2 C_z^2 + 2\mathbb{E}_{\zeta\sim\mu_\mathcal{T}}[\|\mathcal{E}_\eta^*(\zeta)\|^2].$$

Substituting C_z and $R_{\mathcal{T}^*}$, we obtain (36). □

This theorem extends our analysis to the uncertain system (27), which includes model uncertainties and sensor noise. It shows that the expected steady-state error is additively composed of two terms: a learning-dependent term and a design-dependent term. The learning-dependent term $R_{\mathcal{T}^*}$ is the approximation error for the learned inverse map $\hat{\mathcal{T}}_\eta^*$, which we can control via the learning process (Theorem 14). The design-dependent term depends on the noise bounds $(\overline{w}, \overline{v})$ and the observer's design parameters (A, B, ℓ_η). This term can be minimized by choosing A to be

stable ($|\lambda_{\min}(A)|$ large) and well-conditioned ($\text{cond}(V)$ small [6]), and by regularizing the learning of $\hat{\mathcal{T}}_\eta^*$ to keep ℓ_η small. This provides a quantitative link between learning, observer design, and the estimation performance.

8 Simulation Results

In this section, we demonstrate the effectiveness of our proposed methodology [7] for the learning-based design of KKL observers using the following examples:

- *Reverse Duffing oscillator* with state $x \in \mathbb{R}^2$:

$$\dot{x}_1 = x_2^3, \quad \dot{x}_2 = -x_1, \quad y = x_1. \tag{37}$$

- *Van der Pol oscillator* with state $x \in \mathbb{R}^2$ and parameter $\mu = 3$:

$$\dot{x}_1 = x_2, \quad \dot{x}_2 = \mu(1 - x_1^2)x_2 - x_1, \quad y = x_1. \tag{38}$$

- *Rössler attractor* with state $x \in \mathbb{R}^3$ and parameters $a = b = 0.2$ and $c = 5.7$:

$$\begin{aligned} \dot{x}_1 &= -x_2 - x_3, & \dot{x}_2 &= x_1 + ax_2 \\ \dot{x}_3 &= b + x_3(x_1 - c), & y &= x_2. \end{aligned} \tag{39}$$

- *Lorenz attractor* with state $x \in \mathbb{R}^3$ and parameters $p = 28$, $q = 10$, and $r = 8/3$:

$$\begin{aligned} \dot{x}_1 &= p(x_2 - x_1), \ \dot{x}_2 = x_1(q - x_3) - x_2 \\ \dot{x}_3 &= x_1x_2 - rx_3, \ y = x_2. \end{aligned} \tag{40}$$

Using the benchmark examples listed above, we show the effectiveness of our method in estimating the states of nonlinear, chaotic systems in the presence of model uncertainties and measurement noise.

8.1 Experimental Setup

We generate synthetic datasets S_1 and S_2 according to the procedure described in Sections 5.2 and 5.3, and train neural networks for each of the systems (37)–(40) according to our proposed methodology in Section 5. For all systems, we construct the dataset S_1 by uniformly sampling initial conditions over $[-1, 1]^{n_x}$, with n_x denoting the system dimension, which is 2 and 3 for (37)–(38) and (39)–(40), respectively. We sample 100 initial conditions for (37)–(38), while we used 200 samples for (39)–(40). From each sampled initial condition, we generate system trajectories over a time interval of $[0, 50]$ with sampling time 0.1. The truncation sample k_* is set to 0.1τ (10% of the z-trajectory length), which is sufficient to ensure that the effects of all initial conditions vanish by $\varepsilon = 10^{-4}$. The observer matrices $A = \text{diag}(\lambda_1, \ldots, \lambda_{n_z})$, where $\lambda_i \in [-2, -0.5]$ are distinct, and $B = \mathbf{1}_{n_z}$, where $\mathbf{1}_{n_z}$ is a vector of ones.

We model the forward map $\hat{\mathcal{T}}_\theta$ and the inverse map $\hat{\mathcal{T}}_\eta$ as multi-layer perceptions, trained using the synthetic datasets generated for each system. The hyperparameter specifications for each model are presented in Table 1.

[6] For instance, when A is a diagonal matrix, we have $V = I_{n_z}$ and $\text{cond}(V) = 1$.
[7] Our code: `github.com/Mudhdhoo/PINN_KKL`

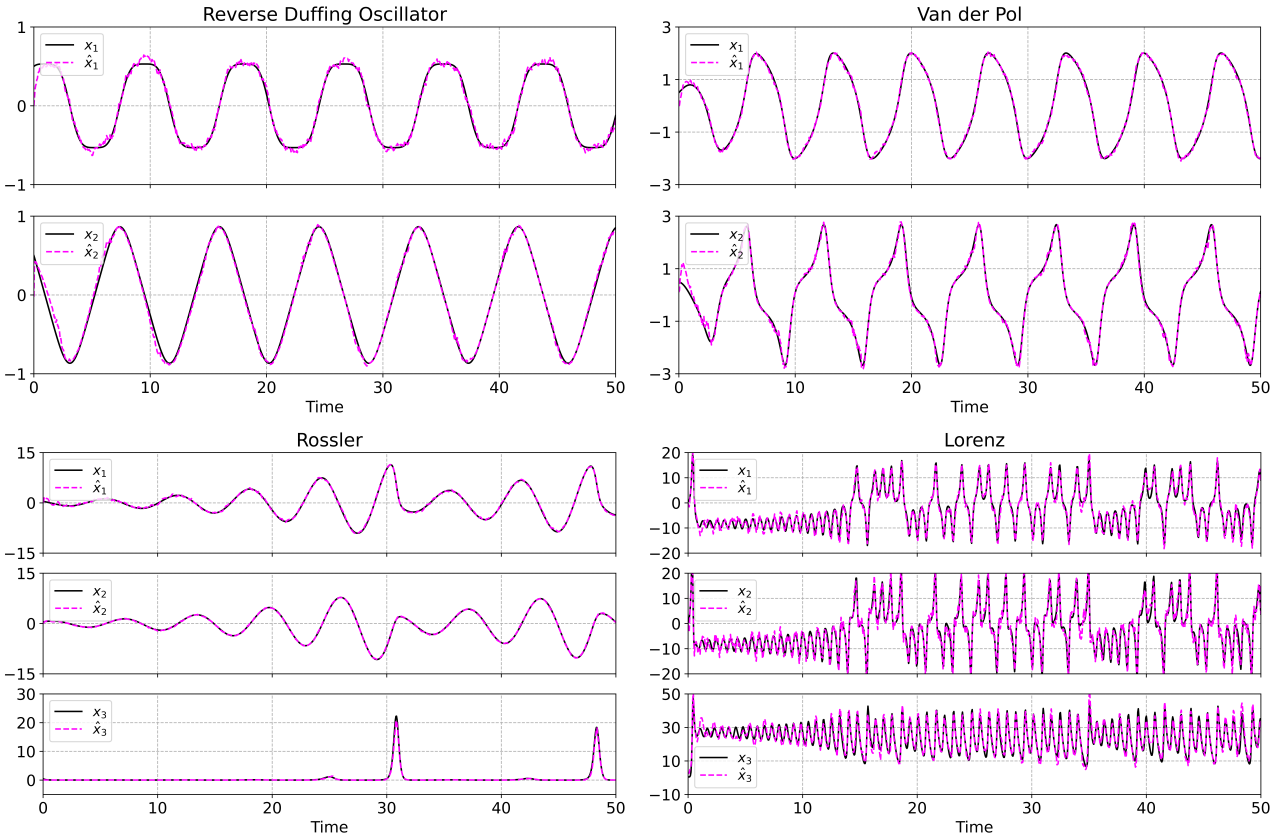

Fig. 2. State estimation with learned KKL observer under noisy measurements. The solid black line shows the true state trajectory, while the dashed magenta line is the state estimate obtained from the learned KKL observer.

Table 1
Hyperparameters used for training. All values are used for both the forward map $\hat{\mathcal{T}}_\theta$ and the inverse map $\hat{\mathcal{T}}_\eta^\star$.

System	**Hidden Layers**	**Layer Size**	**Learning Rate**	**Physics weight ν**	**Epochs**
Duffing	3	150	1×10^{-3}	1	15
VdP	2	350	1×10^{-3}	1	15
Rössler	3	250	1×10^{-3}	1	15
Lorenz	2	350	1×10^{-3}	1	15

8.2 Estimation Results under Measurement Noise

Simulation results for each system are illustrated in Fig. 2. Each trajectory is generated from random initial condition, different from those in the dataset S_1 but sampled within the same region. Each component of the measurement noise is sampled from $\mathcal{N}(0, 0.1)$ for the reverse Duffing oscillator, van der Pol oscillator, and Rössler attractor. In contrast, for the Lorenz attractor, it is sampled from $\mathcal{N}(0, 2)$. In all cases, the observer's initial condition $\hat{z}(0) = 0$. The simulations demonstrate the capability of our method to estimate the state with remarkable accuracy even in the presence of measurement noise.

8.3 Comparison with the State-of-the-Art

We compare the state estimation performance of our sequential learning PINN method (referred to as SPINN) with three established learning-based approaches:

- The unsupervised autoencoder method [8] (AE) with gain tuning proposed by [15]. This is a joint encoder-decoder structure trained in an unsupervised way, with explicit tuning of the observer gain.
- The neural ODE method [9] (NODE) proposed by [36]. This method simultaneously learns the unknown nonlinear system dynamics and the KKL transformation map using a neural ODE structure.
- The deep model-free switching method [10] (DMF) proposed by [42].

The benchmark system is the reverse Duffing oscillator (37). We use the same neural network architecture and hyperparameters (described in Section 8.1 and Table 1) for all methods to ensure a fair comparison and focus solely on the differences in the learning method. We also assess the training costs of each method, which is a critical factor for scalability and rapid prototyping.

In this comparison, we evaluate the generalization capabilities of the learned observers produced by these methods. All methods are trained on data generated in the set $[-1, 1]^{n_x}$. Generalization performance is evaluated by testing over 100 independent trials with initial states of system 37 sampled from a larger set $[-3, 3]^{n_x}$, which the neural networks did not see during training. Recall that $x(t)$ is the true state and $\hat{x}(t)$ is the estimated state. We use two standard metrics to quantify the estimation accuracy across the $N_{\text{traj}} = 100$ independent test trajectories with the number of time samples N_{steps}:

- Root Mean Square Error
$$\text{RMSE} = \sqrt{\frac{1}{N_{\text{traj}} N_{\text{steps}}} \sum_{j=1}^{N_{\text{traj}}} \sum_{t=1}^{N_{\text{steps}}} \|x_j(t) - \hat{x}_j(t)\|^2}$$
measures the absolute magnitude of the average error.
- Symmetric Mean Absolute Percentage Error
$$\text{SMAPE} = \frac{1}{N_{\text{traj}} N_{\text{steps}}} \sum_{j=1}^{N_{\text{traj}}} \sum_{t=1}^{N_{\text{steps}}} \frac{2\|x_j(t) - \hat{x}_j(t)\|}{\|x_j(t)\| + \|\hat{x}_j(t)\|} \times 100\%$$
measures the relative estimation error for comparing accuracy across different scales.

Fig. 3 illustrates a single instance of the estimation performance when the system is initialized outside the training domain. It visually confirms that our observer estimates the state with the best accuracy even when the system is initialized from $[-3, 3]^{n_x}$, which is larger than the training domain. On the other hand, Fig. 4 presents the quantitative error metrics for the 100 test trials. The results show that the generalization performance of our method (SPINN) is significantly better than all other methods in this out-of-domain generalization test.

The observed performance hierarchy yields key insights into the value of physics-informed learning. Our method achieves the best generalization because it (a) explicitly incorporates the PDE constraint in (16), which acts as a physically consistent inductive bias avoiding overfitting on training data, and (b) capitalizes on the sequential decoupling, which improves learning by avoiding the conflicting gradients inherent in joint $\hat{\mathcal{T}}_\theta$ and $\hat{\mathcal{T}}_\eta^*$ training. The PDE (6) is incorporated into neural network training via automatic differentiation and the known system model $f(x)$, thereby reducing the size of the hypothesis space and reliably facilitating extrapolation into unseen state regions. This observation validates the theoretical arguments of Section 6.

[8] Code: `github.com/Centre-automatique-et-systemes/learn_observe_KKL`.
[9] Code: `github.com/KYMiao/L4DC_Neural_ODEs_Observer`
[10] Code: `github.com/jolindien-git/DeepKKL/tree/main/L4DC_2024`

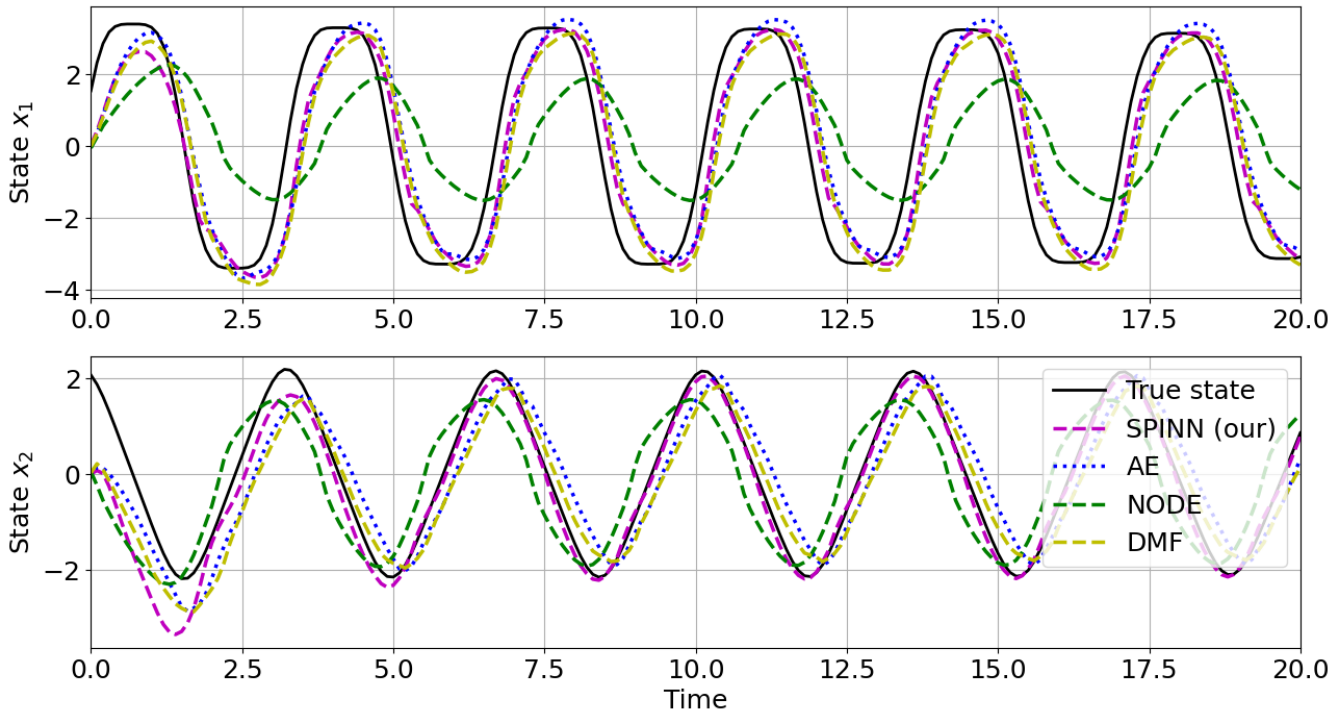

Fig. 3. Estimation performance of KKL observers learned from different methods when the system is initialized outside the training domain.

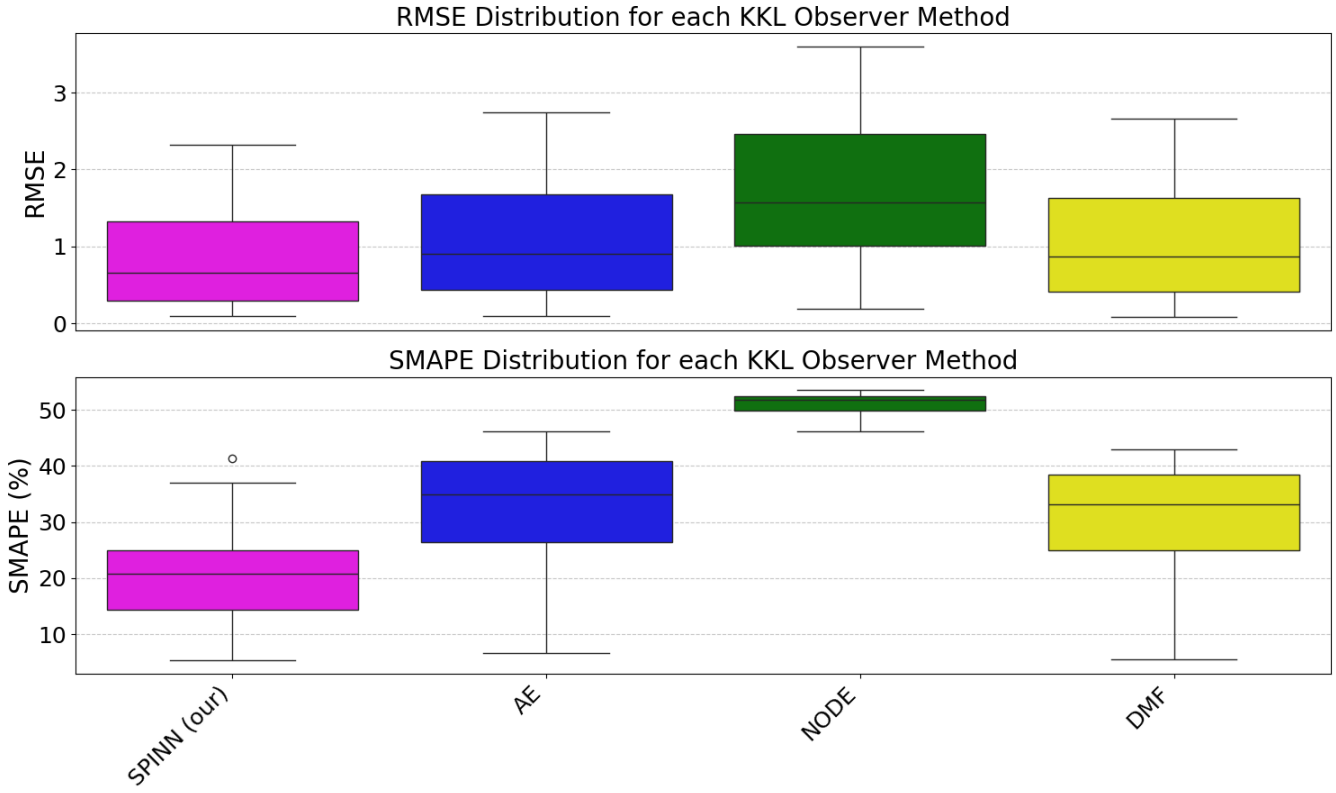

Fig. 4. Comparison of quantitative error metrics averaged over the 100 trials.

Table 2
Computational times for training.

Method	Training Time (s)	Relative Cost	Computational Bottleneck
SPINN (our)	18.29	1x	Sequential procedure and computation of PDE Jacobian $\nabla_x \hat{\mathcal{T}}$
AE	7.68	0.42x	Simple regression
NODE	219.97	12.03x	Numerical ODE integration per forward pass
DMF	7.69	0.42x	Simple regression

The unsupervised AE [15] and DMF [42] methods also exhibit reasonable generalization performance. NODE [36] performs relatively worse in this test. This is because it handles unknown dynamics simultaneously with the unknown state. Since the system model is learned from limited training data in the domain $[-1, 1]^{n_x}$ without any physics knowledge guiding the training in the hypothesis space, the learned model fails to generalize when tested on the unseen domain $[-3, 3]^{n_x}$. This model identification error, in turn, contaminates the observer's performance. Note that it is an expected limitation of simultaneous model identification and state estimation in a limited-data regime. On the other hand, the DMF method [42], which is also model-free, benefits from a streamlined learning objective that directly targets the KKL injectivity property, without inheriting the costly burden of learning the system dynamics from data.

All models were trained on a MacBook Pro equipped with the Apple M3 Max, featuring a 16-core CPU (12 performance cores and 4 efficiency cores) and a 40-core GPU. The system utilizes 128 GB of unified memory with a memory bandwidth of 400 GB/s. The total training times for the 15 epochs (or equivalent iterations) are reported in Table 2. The unsupervised AE [15] and deep model-free [42] methods are the most efficient ($\sim$7.7s). Their objective functions rely solely on algebraic reconstruction losses, allowing for extremely fast backpropagation. Our method (SPINN) required approximately 2.4$\times$ ($\sim$18.3s) the training time of these methods. This overhead is the direct cost of the physics-informed constraint: evaluating the PDE residual requires computing the Jacobian $\frac{\partial \hat{\mathcal{T}}}{\partial x}$ via automatic differentiation at every step. However, this cost is constant and leads to the significant generalization gains observed in Fig. 4. The neural ODE method [36] is orders of magnitude slower ($\sim$220s). This is because every forward pass of the network requires a numerical ODE solver to integrate the learned neural ODE dynamics over time. Backpropagating through this solver (or using the adjoint method) is computationally expensive, making the NODE method less suitable for scenarios that require rapid retraining or real-time adaptation.

9 Conclusion

We proposed a learning-based method for designing KKL observers for autonomous nonlinear systems. We trained neural networks using synthetically generated data to approximate the transformation map and its inverse, which are required for synthesizing a KKL observer. Instead of simultaneously learning the transformation and its inverse, we proposed learning them sequentially to avoid conflicting gradients during training and improve accuracy. First, the transformation map is learned by a physics-informed neural network that incorporates the PDE associated with the KKL observer via automatic differentiation. Then, by generating new data and using the learned transformation map to produce corresponding features, a second neural network learns the inverse map by minimizing the empirical reconstruction risk.

Theoretically, we provided non-asymptotic generalization bounds for the learned KKL observer. We proved that minimizing the empirical risk guarantees the input-to-state stability of the state estimation error with respect to approximation errors and system uncertainties. The effectiveness of our approach was validated through comprehensive state estimation experiments across multiple benchmark systems. We demonstrated the generalization capability of

the learned KKL observer by comparing it with the state-of-the-art methods. The excellent performance is due to that the PDE constraint serves as a physically consistent inductive bias that effectively reduces the hypothesis space for neural networks, enabling extrapolation where purely data-driven methods fail.

Our future research will address some key open problems. The primary challenge lies in extending KKL observer learning to non-autonomous and controlled nonlinear systems, where the transformation maps and their inverses are time-varying. This temporal dependency results in time-dependent PDEs that probably require more complex neural network architectures. Moreover, combining PINNs for system identification with observer design would address the unknown system model scenario more robustly than current end-to-end learning methods. Finally, we will also explore active learning to identify where in the state space the PDE residual is high and sample adaptively from those regions, further reducing the data requirement.

Acknowledgements

This work is supported by the European Union's Horizon Research and Innovation Programme under Marie Skłodowska-Curie grant agreement No. 101062523. It has also received funding from the Swedish Research Council's Distinguished Professor Grant and the Knut and Alice Wallenberg Foundation's Wallenberg Scholar Grant.

References

[1] M. Abudia, J. A. Rosenfeld, and R. Kamalapurkar. Carleman lifting for nonlinear system identification with guaranteed error bounds. In *American Control Conference (ACC)*, pages 929–934, 2023.

[2] V. Andrieu. Convergence speed of nonlinear Luenberger observers. *SIAM Journal on Control and Optimization*, 52(5):2831–2856, 2014.

[3] V. Andrieu and P. Bernard. Remarks about the numerical inversion of injective nonlinear maps. In *60th IEEE Conference on Decision and Control (CDC)*, pages 5428–5434, 2021.

[4] V. Andrieu and L. Praly. On the existence of a Kazantzis–Kravaris/Luenberger observer. *SIAM Journal on Control and Optimization*, 45(2):432–456, 2006.

[5] P. J. Antsaklis and A. N. Michel. *A Linear Systems Primer*. Springer Birkhäuser Boston, MA, 2007.

[6] P. Ashwin and J. Newman. Physical invariant measures and tipping probabilities for chaotic attractors of asymptotically autonomous systems. *The European Physical Journal Special Topics*, 230(16):3235–3248, 2021.

[7] F. Bach. *Learning Theory from First Principles*. MIT Press, 2024.

[8] P. Bernard. Luenberger observers for nonlinear controlled systems. In *56th IEEE Conference on Decision and Control (CDC)*, pages 3676–3681, 2017.

[9] P. Bernard. *Observer Design for Nonlinear Systems*, volume 479. Springer, 2019.

[10] P. Bernard and V. Andrieu. Luenberger observers for nonautonomous nonlinear systems. *IEEE Transactions on Automatic Control*, 64(1):270–281, 2018.

[11] P. Bernard, V. Andrieu, and D. Astolfi. Observer design for continuous-time dynamical systems. *Annual Reviews in Control*, 53:224–248, 2022.

[12] P. Bernard and M. Maghenem. Reconstructing indistinguishable solutions via a set-valued KKL observer. *Automatica*, 166:111703, 2024.

[13] D. Boutat and G. Zheng. *Observer Design for Nonlinear Dynamical Systems*. Springer, 2021.

[14] L. Brivadis, V. Andrieu, P. Bernard, and U. Serres. Further remarks on KKL observers. *Systems & Control Letters*, 172:105429, 2023.

[15] M. Buisson-Fenet, L. Bahr, V. Morgenthaler, and F. Di Meglio. Towards gain tuning for numerical KKL observers. *IFAC-PapersOnLine*, 56(2):4061–4067, 2023.

[16] J. Cao, M. U. B. Niazi, M. Barreau, and K. H. Johansson. Sensor fault detection and isolation in autonomous nonlinear systems using neural network-based observers. In *European Control Conference (ECC)*, pages 7–12, 2024.

[17] B. Chen and G. Hu. Nonlinear state estimation under bounded noises. *Automatica*, 98:159–168, 2018.

[18] W. Chen and M. Saif. Observer-based strategies for actuator fault detection, isolation and estimation for certain class of uncertain nonlinear systems. *IET Control Theory & Applications*, 1(6):1672–1680, 2007.

[19] F. Dettù, S. Formentin, and S. Matteo Savaresi. Joint vehicle state and parameters estimation via twin-in-the-loop observers. *Vehicle System Dynamics*, 62(9):2423–2449, 2024.

[20] Y. Ebihara, X. Dai, T. Yuno, V. Magron, D. Peaucelle, and S. Tarbouriech. Local Lipschitz constant computation of ReLU-FNNs: Upper bound computation with exactness verification. In *European Control Conference (ECC)*, pages 2506–2511, 2024.

[21] J.-P. Eckmann and D. Ruelle. Ergodic theory of chaos and strange attractors. *Reviews of Modern Physics*, 57(3):617, 1985.

[22] R. Engel. Nonlinear observers for Lipschitz continuous systems with inputs. *International Journal of Control*, 80(4):495–508, 2007.

[23] M. Fazlyab, A. Robey, H. Hassani, M. Morari, and G. Pappas. Efficient and accurate estimation of Lipschitz constants for deep neural networks. *Advances in Neural Information Processing Systems*, 32, 2019.

[24] J.-P. Gauthier and I. Kupka. *Deterministic Observation Theory and Applications*. Cambridge University Press, 2001.

[25] D. Haussler. Decision theoretic generalizations of the PAC model for neural net and other learning applications. *Information and Computation*, 100(1):78–150, 1992.

[26] M. Jordan and A. G. Dimakis. Exactly computing the local Lipschitz constant of ReLU networks. *Advances in Neural Information Processing Systems*, 33:7344–7353, 2020.

[27] N. Kazantzis and C. Kravaris. Nonlinear observer design using Lyapunov's auxiliary theorem. *Systems & Control Letters*, 34(5):241–247, 1998.

[28] H. K. Khalil and L. Praly. High-gain observers in nonlinear feedback control. *International Journal of Robust and Nonlinear Control*, 24(6):993–1015, 2014.

[29] G. Kreisselmeier and R. Engel. Nonlinear observers for autonomous Lipschitz continuous systems. *IEEE Transactions on Automatic Control*, 48(3):451–464, 2003.

[30] A. J. Krener and M. Xiao. Nonlinear observer design in the Siegel domain. *SIAM Journal on Control and Optimization*, 41(3):932–953, 2002.

[31] L. Ljung. *System Identification: Theory for the User*. Prentice-Hall, Upper Saddle River, NJ, 2nd edition, 1999.

[32] D. Luenberger. Observing the state of a linear system. *IEEE Transactions on Military Electronics*, 8(2):74–80, 1964.

[33] D. Luenberger. Observers for multivariable systems. *IEEE Transactions on Automatic Control*, 11(2):190–197, 1966.

[34] D. Luenberger. An introduction to observers. *IEEE Transactions on Automatic Control*, 16(6):596–602, 1971.

[35] H. Mania, M. I. Jordan, and B. Recht. Active learning for nonlinear system identification with guarantees. *Journal of Machine Learning Research*, 23:1–30, 2022.

[36] K. Miao and K. Gatsis. Learning robust state observers using neural ODEs. In *Learning for Dynamics and Control Conference*, pages 208–219, 2023.

[37] M. Milanese, J. Norton, H. Piet-Lahanier, and É. Walter. *Bounding Approaches to System Identification*. Springer New York, NY, 1996.

[38] M. Mohri, A. Rostamizadeh, and A. Talwalkar. *Foundations of Machine Learning*. MIT press, 2018.

[39] M. U. B. Niazi, J. Cao, X. Sun, A. Das, and K. H. Johansson. Learning-based design of Luenberger observers for autonomous nonlinear systems. In *American Control Conference (ACC)*, pages 3048–3055, 2023.

[40] V. Pachy, V. Andrieu, P. Bernard, L. Brivadis, and L. Praly. On the existence of KKL observers with nonlinear contracting dynamics. *IFAC-PapersOnLine*, 58(21):262–267, 2024.

[41] J. Peralez and M. Nadri. Deep learning-based Luenberger observer design for discrete-time nonlinear systems. In *60th IEEE Conference on Decision and Control (CDC)*, pages 4370–4375, 2021.

[42] J. Peralez and M. Nadri. Deep model-free KKL observer: A switching approach. In *Learning for Dynamics and Control Conference*, pages 929–940, 2024.

[43] D. Pollard. *Empirical Processes: Theory and Applications*. Institute of Mathematical Statistics, 1990.

[44] L. d. C. Ramos, F. Di Meglio, V. Morgenthaler, L. F. F. da Silva, and P. Bernard. Numerical design of Luenberger observers for nonlinear systems. In *59th IEEE Conference on Decision and Control (CDC)*, pages 5435–5442, 2020.

[45] A. Shoshitaishvili. Singularities for projections of integral manifolds with applications to control and observation problems. In *Theory of Singularities and its Applications*, pages 295–333. American Mathematical Society, 1990.

[46] A. Shoshitaishvili. On control branching systems with degenerate linearization. In *IFAC Symposium on Nonlinear Control Systems*, pages 495–500, 1992.

[47] E. D. Sontag. *Mathematical Control Theory: Deterministic Finite Dimensional Systems*, volume 6. Springer New York, NY, 2nd edition, 2013.

[48] C. Szegedy, W. Zaremba, I. Sutskever, J. Bruna, D. Erhan, I. Goodfellow, and R. Fergus. Intriguing properties of neural networks. *arXiv preprint arXiv:1312.6199*, 2013.

[49] A. Teel and L. Praly. Tools for semiglobal stabilization by partial state and output feedback. *SIAM Journal on Control and Optimization*, 33(5):1443–1488, 1995.

[50] G. Q. B. Tran and P. Bernard. Arbitrarily fast robust KKL observer for nonlinear time-varying discrete systems. *IEEE Transactions on Automatic Control*, 69(3):1520–1535, 2023.

[51] V. Vapnik and A. Y. Chervonenkis. On the uniform convergence of relative frequencies of events to their probabilities. *Theory of Probability & Its Applications*, 16(2):264–280, 1971.

[52] A. Virmaux and K. Scaman. Lipschitz regularity of deep neural networks: Analysis and efficient estimation. *Advances in Neural Information Processing Systems*, 31, 2018.

[53] L.-S. Young. What are SRB measures, and which dynamical systems have them? *Journal of Statistical Physics*, 108(5):733–754, 2002.